

Mineralogy and diagenesis of Mars-analog paleosols from eastern Oregon, USA

Adrian P. Broz^{a,*}, Joanna Clark^b, Brad Sutter^c, Doug W. Ming^d, Valerie Tu^c, Briony Horgan^e, Lucas C.R. Silva^f

^a Department of Earth Sciences, University of Oregon, Eugene, OR 97405, United States of America

^b Geocontrols Systems – Jacobs JETS Contract, NASA Johnson Space Center, Houston, TX 77058, United States of America

^c Jacobs JETS Contract, NASA Johnson Space Center, Houston, TX 77058, United States of America

^d NASA Johnson Space Center, Houston, TX 77058, United States of America

^e Department of Earth, Atmospheric and Planetary Science, Purdue University, IN, 47907, United States of America

^f Environmental Studies Program, Department of Geography, University of Oregon, Eugene, OR 97405, United States of America

ARTICLE INFO

Keywords:

Pedogenesis
Martian paleosols
Weathering profiles
SAM-EGA
VNIR spectroscopy

ABSTRACT

Ancient (4.1–3.7-billion-year-old) layered sedimentary rocks on Mars are rich in clay minerals which formed from aqueous alteration of the Martian surface. Many of these sedimentary rocks appear to be composed of vertical sequences of Fe/Mg clay minerals overlain by Al clay minerals that resemble paleosols (ancient, buried soils) from Earth. The types and properties of minerals in paleosols can be used to constrain the environmental conditions during formation to better understand weathering and diagenesis on Mars. This work examines the mineralogy and diagenetic alteration of volcanoclastic paleosols from the Eocene-Oligocene (43–28 Ma) Clarno and John Day Formations in eastern Oregon as a Mars-analog site. Here, paleosols rich in Al phyllosilicates and amorphous colloids overlie paleosols with Fe/Mg smectites that altogether span a sequence of ~ 500 individual profiles across hundreds of meters of vertical stratigraphy. Samples collected from three of these paleosol profiles were analyzed with visible/near-infrared (VNIR) spectroscopy, X-ray diffraction (XRD), and evolved gas analysis (EGA) configured to operate like the SAM-EGA instrument onboard *Curiosity* Mars Rover. Strongly crystalline Al/Fe dioctahedral phyllosilicates (montmorillonite and nontronite) were the major phases identified in all samples with all methods. Minor phases included the zeolite mineral clinoptilolite, as well as andesine, cristobalite, opal-CT and gypsum. Evolved H₂O was detected in all samples and was consistent with adsorbed water and the dehydroxylation of a dioctahedral phyllosilicate, and differences in H₂O evolutions between montmorillonite and nontronite were readily observable. Detections of hematite and zeolites suggested paleosols were affected by burial reddening and zeolitization, but absence of illite and chlorite suggest that potash metasomatism and other, more severe diagenetic alterations had not occurred. The high clay mineral content of the observed paleosols (up to 95 wt%) may have minimized diagenetic alteration over geological time scales. Martian paleosols rich in Al and Fe smectites may have also resisted severe diagenetic alteration, which is favorable for future in-situ examination. Results from this work can help differentiate paleosols and weathering profiles from other types of sedimentary rocks in the geological record of Mars.

1. Introduction

Today the surface of Mars is frigid, wind-deflated and barren, but there is extensive geological evidence for transient warm and wet habitable surface conditions in the Noachian (4.1–3.7 Ga) period of early Mars (Bishop et al., 2008a, 2008b; Bishop et al., 2013; Scheller et al., 2021; Ye and Michalski, 2021). Orbital sensing of the Martian surface

has revealed clay mineral deposits in thousands of locations, wherever Noachian-age terrains are not obscured by dust, sand, or overlying strata (Murchie et al., 2007; Carter et al., 2015; Loizeau et al., 2018; Franklin et al., 2021). These ancient deposits are rich in smectite clay minerals and other hydrated phases, suggesting formation in subsurface and surface environments from the weathering of mafic rocks and sediments with liquid water.

* Corresponding author.

E-mail address: abroz@uoregon.edu (A.P. Broz).

<https://doi.org/10.1016/j.icarus.2022.114965>

Received 27 September 2021; Received in revised form 2 February 2022; Accepted 21 February 2022

0019-1035/© 20XX

While some phyllosilicates on Mars are associated with lacustrine deposition in surface environments (e.g., (Bristow et al., 2018)) many phyllosilicate detections occur in regionally widespread deposits, inconsistent with deposition in basin settings. Two hypotheses to explain the formation, occurrence and distribution of these regionally widespread phyllosilicates on Mars are: 1) subsurface hydrothermal activity, diagenesis and/or authigenesis (Ehlmann et al., 2008, 2010; Vaniman et al., 2014; Michalski et al., 2015; Bishop et al., 2018) and, 2) surface pedogenic alteration (e.g., subaerial chemical weathering) (Horgan et al., 2012; Bishop et al., 2013, 2018; Carter et al., 2015). In some locations, trioctahedral smectites exhibiting lateral variations in Al and Fe/Mg smectites intermixed with chlorite, serpentinite, talc and zeolite are consistent with formation in hydrothermal subsurface environments, diagenesis, and/or authigenesis during sediment emplacement (Ehlmann et al., 2011; Vaniman et al., 2014; Cannon et al., 2017). However, dioctahedral smectites often outcrop as extensive vertical profiles of Fe/Mg smectites overlain by Al smectites, suggesting subaerial formation in surface environments, consistent with pedogenesis (soil formation) or large-scale leaching of sediments (Bishop et al., 2018).

Paleosols are ancient, buried soils that are lithified into sedimentary rocks. On Earth, paleosols are a geological record of the atmospheric composition, climate, topography and organisms present before soil burial (Retallack, 2019). Paleosols are created by removal from their soil-forming factors, sometimes because of change in those factors, but most often by rapid burial. The deposition of volcanic ash, flood basalts, sedimentation from flooding, landslides, and tsunamites all rapidly bury surface environments. Sequences of paleosols form when soils are periodically buried, for example by repeated volcanic eruptions which emplace tephra or lava onto soil surfaces, followed by successive pedogenic weathering of emplaced tephra or lava, and then subsequent burial by another eruption. Flooding by rivers also buries paleosols within alluvial sequences, and dune migration buries paleosols within eolian sequences. On Earth, sequences of paleosols formed by periodic burial can record weathering, paleoclimate and diagenetic alteration over 10^7 year timescales (Horgan, 2016; Smith and Horgan, 2021).

Paleosols can be useful tools for interpreting ancient climates of Earth and Mars (Rye et al., 2000; Heard and Kite, 2020; Heard et al., 2021). The types and properties of minerals in analog paleosols from Earth can be used to help understand the nature of weathering and diagenesis on Mars (Retallack, 2014; Liu et al., 2021a) but they remain relatively understudied as Mars-analog sites. A principal question of this research is whether the mineralogy and diagenetic alteration of terrestrial paleosols can be identified using techniques relevant to Mars exploration. The objective of this study was to determine the mineralogy and diagenetic alteration of Mars-analog paleosols from eastern Oregon, USA using analytical techniques similar to those onboard current and future missions to Mars.

1.1. Paleosols at John Day fossil beds national monument

The John Day Fossil Beds National Monument in eastern Oregon, USA, is an established Mars-analog site. It is known for similarities in mineralogy and stratigraphy to clay-bearing sedimentary rocks on Mars (Horgan, 2016; Hays et al., 2017; Lantz et al., 2020). Here, Eocene and Oligocene (42–28 Ma) sedimentary rocks are a well-preserved sequence of andesitic to rhyodacitic paleosols (Bestland, 1997; Retallack et al., 2000; Horgan et al., 2012; Smith et al., 2018a). The ~400-m-thick sequence is host to over 500 individual clay mineral-rich (30–95 wt%) paleosols spanning 15 Myr through the climatic cooling of the Eocene-Oligocene boundary (Fig. 1). A record of dramatic climate change is preserved in the mineralogy of paleosols from the Eocene/Oligocene-age Clarno and John Day Formations, transitioning from high kaolinite and oxide abundances at the bottom (warm and wet Eocene), to high smectite abundances (drying out late Eocene), and then poorly crys-

talline phases at the stratigraphic top of the section (cool and dry Oligocene) (Bestland, 1997; Retallack et al., 2000).

Stratigraphically lowest in the section are deeply weathered red and purple lateritic paleosols (Oxisols and Ultisols in US Taxonomy (Soil Survey Staff, 2014) within the uppermost Clarno and lowermost John Day Formations in the Painted Hills (~42 Ma). These paleosols formed under a warm and wet climate of an estimated 900–2000 mm mean annual precipitation (MAP) and mean annual temperature (MAT) of 23–25 °C (Retallack et al., 2000) (Fig. 2). The Clarno paleosols have accumulations of oxides, kaolinite, and Fe/Mg smectite. They are erosionally truncated and abruptly overlain by less deeply weathered Al/Fe smectite-rich paleosols (Inceptisols and Alfisols) of the middle Big Basin Member of the John Day Formation (~33 Ma). This truncation surface is correlated with the international Eocene-Oligocene boundary (Retallack et al., 2000). Big Basin member soils appear to have formed under a markedly cooler (MAT 16–18 °C) and drier (MAP 600–1200 mm) climate relative to the early Eocene (Sheldon et al., 2002). Stratigraphically above, in the Turtle Cove (TC) paleosols, another erosional truncation marks the base of the late Oligocene (~28 Ma) lower Turtle Cove Member of the John Day Formation which has minimally weathered calcareous paleosols (Aridisols and Andisols) containing abundant celadonite, calcite and amorphous colloids (imogolite, ferrihydrite and allophane) which indicate an even drier (MAP 400–600 mm) climate during the late Oligocene (Bestland, 2002).

The Turtle Cove Member (late Oligocene) is composed of light brown and green colored Andisol (volcanic soils) and Aridisol (desert soils) paleosols that overlie the upper Big Basin member of the John Day Formation. The Turtle Cove Member has increased amounts of amorphous phases and calcite as well as the blue to green-colored clay mineral celadonite. Celadonite in the Turtle Cove paleosols is thought to form from the recrystallization of poorly crystalline smectite and/or amorphous phases (Retallack et al., 2000). Turtle Cove paleosols have a dramatic reduction in smectite abundance and near absence of kaolin-group clays relative to the Clarno Formation paleosols at the base of the section (Retallack et al., 2000; Horgan et al., 2012).

Stratigraphically above the terrestrial Turtle Cove Member paleosols, approximately 300 vertical meters of flood basalts from the Columbia River Group cap the entire sequence. In summary, the Eocene-age paleosols at the base of the section have accumulations of kaolinite and oxides that reflect a subtropical and humid climate, late Eocene/early Oligocene profiles in the middle of the section have Al/Fe smectites associated with a more arid climate, and the uppermost paleosols with nanophase aluminosilicates and amorphous phases indicate step-wise and cooling and drying during the late Oligocene (Retallack et al., 2000).

1.2. Comparisons to putative Martian paleosols

Sequences of paleosols in the Clarno and John Day Formations are similar in mineralogy and stratigraphy to dioctahedral clay mineral sequences at Mawrth Vallis (Horgan et al., 2012; Hays et al., 2017). Remote sensing of the Martian surface has revealed Noachian-age (4.1–3.7 Ga) layered sedimentary rocks rich in dioctahedral clay minerals that appear to be distributed globally across the surface of Mars (Carter et al., 2015; Bishop et al., 2018; Loizeau et al., 2018). These rocks are generally characterized by strong spectral signatures of Al clays overlying Fe/Mg clays over hundreds of vertical meters of stratigraphy. One hypothesis for their formation is from pedogenic weathering of mafic sediments such as volcanic ash during intermittent warm periods early in Mars' history (Le Deit et al., 2012; Carter et al., 2015; Bishop et al., 2018; Liu et al., 2021a). These altered sediments have been detected at topographic highs including the summits and flanks of volcanoes which is consistent with formation in surface environments via pedogenic weathering (Ye and Michalski, 2021). Many of the clear-

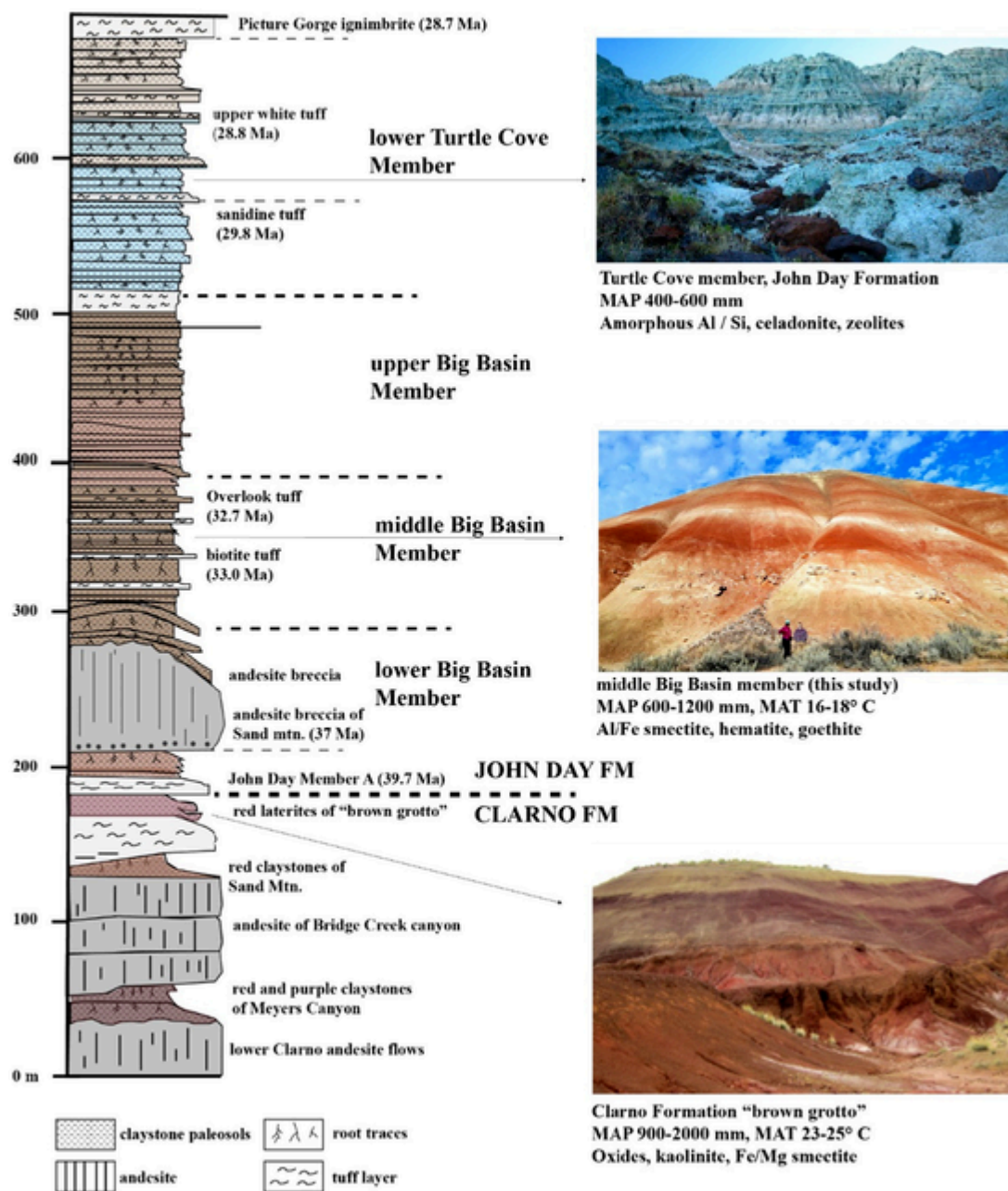


Fig. 1. A sequence of Eocene through Oligocene (43–28 Ma) volcaniclastic paleosols in the Clarno and John Day Formations, John Day Fossil Beds National Monument (redrawn from Bestland, 1997). Mean annual precipitation (MAP) and mean annual temperature (MAT) estimates are from Retallack et al. (2000) and Sheldon et al. (2002).

est examples of putative weathering profiles are observed in crater rims (Horgan et al., 2012; Hays et al., 2017).

The rim of Muara Crater at Mawrth Vallis is host to a 150–200 m thick Fe/Mg smectite unit (topped by sulfate deposits in some areas) overlain by a 50 m-thick Al-phyllsilicate or opal unit which transitions upward into poorly crystalline aluminosilicates or nanophase materials (NOE Dobrea et al., 2010; Lowe et al., 2020). The entire section is then capped by an igneous deposit which appears to be composed of lava and/or basaltic sand (Bishop et al., 2018), similar to the stratigraphy of the John Day Formation paleosols which are capped by approximately 300 m of flood basalts. The basal Fe/Mg clay and oxide unit of the John Day paleosol sequence generally resembles the basal Fe/Mg clay unit at Mawrth Vallis on Mars (Horgan, 2016). In a similar way, the accumulation of amorphous / nanocrystalline phases at stratigraphic top of the Noachian-age section at Mawrth Vallis (Bishop et al., 2020) is consis-

tent with a drier, colder climate that was not sufficient to weather volcanic ash into more crystalline phases, and is analogous to the Oligocene Turtle Cove member of the John Day Formation which contains amorphous phases, hydrated silica, calcite, and celadonite. Spectral signatures of carbonates (Bultel et al., 2019) and celadonite (or glauconite) (Milliken et al., 2008) associated with possible weathering profiles have been noted in the Mawrth Vallis region, but it is currently unclear if celadonite or calcite are indeed components of martian weathering profiles.

Overall, the layering of dioctahedral Al clay minerals and Fe/Mg clay minerals over hundreds of vertical meters suggests a subaerial formation environment for clay minerals in the Mawrth Vallis region (Bishop et al., 2018; Liu et al., 2021a). Congruent pedogenic alteration of basaltic parent material under warm and wet conditions transitioning to more arid conditions is one hypothesis to explain the exceptional

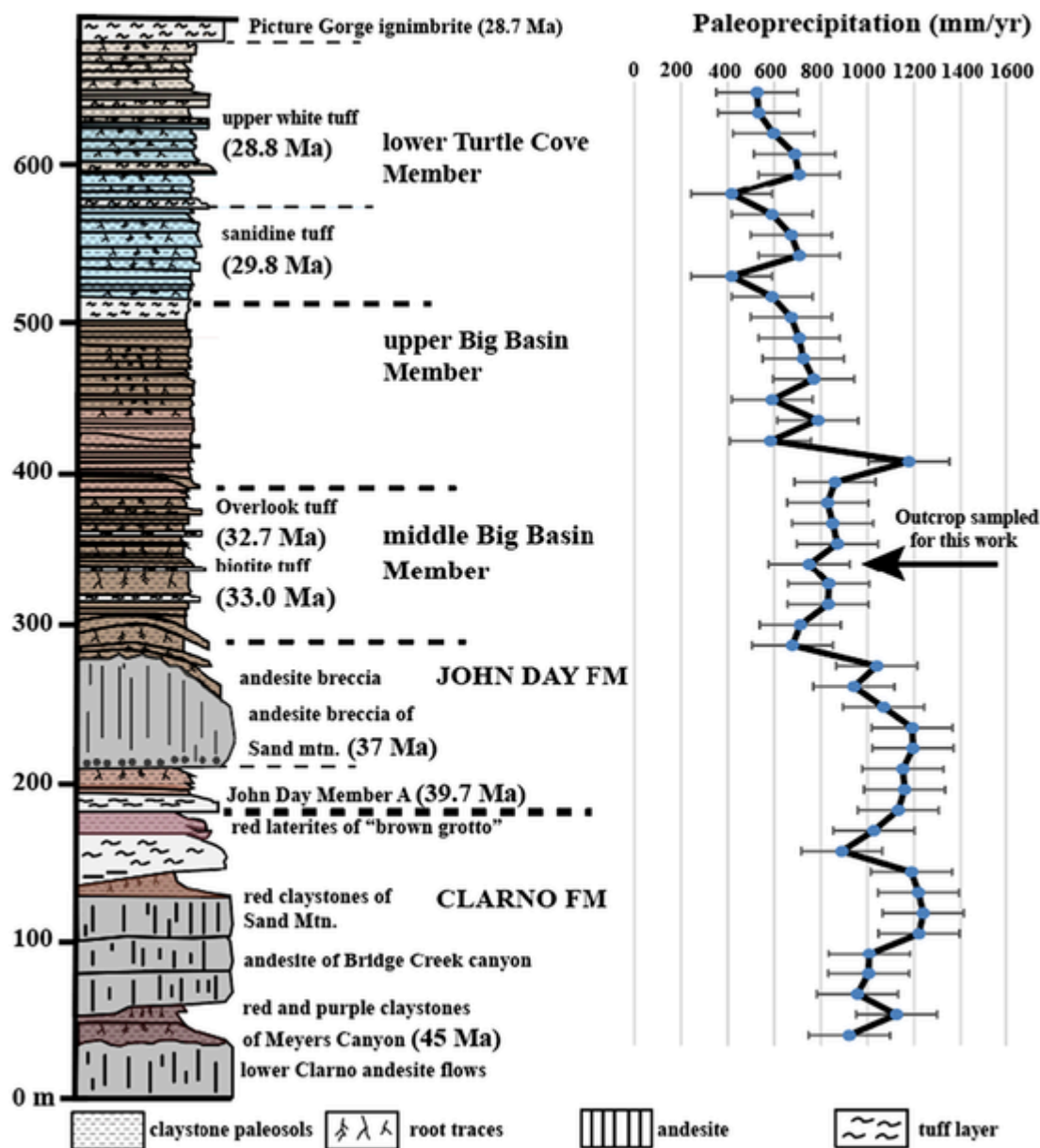


Fig. 2. Previously published paleoprecipitation estimates inferred from the mineralogy of paleosols from the Clarno and John Day Formations (redrawn from Bestland (1997) and Sheldon et al. (2002)). Paleoprecipitation estimates were determined by Retallack et al. (2000) and Sheldon et al. (2002) using an equation relating molecular weathering ratios (Bases/alumina $[\text{CaO} + \text{MgO} + \text{Na}_2\text{O} + \text{K}_2\text{O}] / \text{Al}_2\text{O}_3$) to mean annual precipitation from a database of modern U.S. soils ($r = 0.79$, standard error = 179 mm) (Sheldon et al., 2002). The stratigraphic level of paleosols analyzed in this study is indicated (black arrow).

thickness of the Mawrth Vallis sequence (Horgan et al., 2012; Carter et al., 2015; Loizeau et al., 2015; Bishop et al., 2016).

The compositional stratigraphy at Mawrth Vallis has been proposed to be either a paleosol sequence (Horgan et al., 2012) or a deep weathering profile (e.g., saprolite mantle) (Liu et al., 2021a), which are distinct from one another. Terrestrial paleosol sequences are stacks of individual, meter-scale weathering profiles that form from repeated pedogenic alteration followed by burial. With repeated pedogenic alteration and burial by tephra or lava over 10^6 – 10^7 yr scales, volcanoclastic sequences of individual paleosol profiles can reach hundreds to thousands of meters in vertical thickness (Retallack, 1995; Horgan, 2013; Heard and Kite, 2020). Rapid burial of each paleosol surface via emplacement of tephra or lava can also create favorable conditions for the preservation of biosignatures. In terrestrial settings, each individual profile within the sequence typically accumulates and preserves organic carbon in the near-surface layers, just below the uppermost burial layer

(Broz, 2020), which often presents at field scale as a nonconformity (Retallack, 2019).

By contrast, deep weathering profiles are the products of intense, long-term chemical weathering across tectonically stable landscapes and instead are characterized by a single, massive, and uninterrupted weathering profile. They are most common at terrestrial intertropical latitudes between 35°N and 35°S (Butt et al., 2000). The vertical extent of deep weathering profiles, which includes weathered residuum and sediments overlying basement rocks, varies from a few meters to over 150 m, dependent on climate, tectonic activity, age of the land surface and the properties of the bedrock (Butt et al., 2000; Zauyah et al., 2018). The generally flat-lying topographic relief of deep weathering profiles allows for leaching of weathering products, usually when the downward progression of the weathering front exceeds the erosion rate (Zauyah et al., 2018). The weathering front typically obliterates any primary sedimentary structures such as relict bedding of the basal un-

weathered layers in each profile (C and R horizons in US Soil Taxonomy). The organic preservation potential of terrestrial deep weathering profiles (e.g., laterites) is generally considered to be poor, largely in part due to leaching and/or oxidation of endogenous organic molecules derived from surface biomass (Beukes et al., 2002). However, Noachian (4.1–3.7 Ga) surface weathering may have proceeded under an anoxic atmosphere and was possibly similar in nature to Archean (4.1–2.6 Ga) anoxic pedogenic weathering on Earth. Reducing conditions during ancient pedogenic weathering creates favorable taphonomic conditions for the preservation of biosignatures over geological time scales, including carbonaceous microfossils (Rye et al., 2000) and organic carbon associated with mineral surfaces (Watanabe et al., 2000, 2004). Therefore, distinguishing between paleosol sequences and deep weathering profiles has major implications for paleoclimate interpretations and biosignature preservation in rocks from the compositional stratigraphy within the Mawrth Vallis region (Bishop et al., 2018).

The thickness of the Mawrth Vallis compositional stratigraphy (~150–200 m) appears to also exceed the typical thickness of terrestrial deep weathering profiles (typically less than 100 m). The stratigraphy could have resulted from sediment deposition and then extensive vertical leaching by liquid water during post-depositional diagenesis, but such deep leaching profiles on Earth rarely exceed 150 m in thickness (Horgan et al., 2012). The exposed stratigraphy at Mawrth Vallis also appears to have lateral and vertical diversity beyond the overall Fe/Mg smectite – Al–Si phase stratigraphy (Horgan et al., 2012). Lateral and vertical diversity of clay minerals is not found in deep weathering profiles but is common in paleosols, which have diversity in composition and color at ~1-m scales. The 18 m/pixel resolution of CRISM (Murchie et al., 2007) may limit interpretations of the mineralogical diversity of these deposits on Mars because the fine-scale features within individual paleosol profiles may be obscured at these resolutions.

There also appears to be relict bedding of dark-toned materials throughout the deposit, which suggests the coarse-sized fraction of the parent material may be preserved in certain layers as less-weathered bottom layers (C and R horizons) of paleosols. This relict bedding would presumably be destroyed if the entire deposit was a deep weathering profile (Horgan et al., 2012). Dioctahedral phyllosilicate layers at Mawrth Vallis may be a paleosol sequence that formed under a semi-arid climate, overlain by a thinner leaching profile and capped by a relatively unaltered igneous deposit (Horgan, 2016; Horgan et al., 2017a). This stratigraphy is consistent with climate hypotheses for early Mars, including a Noachian hyperarid frigid paleoclimate alternating with warmer and wetter conditions (Retallack, 2014; Bishop et al., 2018). A similar pedogenic-like stratigraphy of dioctahedral Al clays overlying Fe/Mg clays has been detected in hundreds of locations across the surface of Mars which suggests widespread surface weathering was not limited to the Mawrth Vallis region (Carter et al., 2015; Loizeau et al., 2018). The mid-Noachian Fe/Mg clay unit at Oxia Planum, where the ExoMars 2022 *Rosalind Franklin* rover will land, is thought to be an extension of the lowermost parts of the stratigraphy at Mawrth Vallis (Quantin et al., 2016), and may represent the oldest terrains on Mars ever explored by a landed mission (Quantin-Nataf et al., 2021). Since some of the layered clay mineral sequences on Mars resemble terrestrial paleosols (Liu et al., 2021b), a detailed mineralogical analysis of paleosols from Earth can help with identification and interpretation of these deposits. This study seeks to determine if pedogenic and diagenetic features in ancient terrestrial samples can be identified with a multi-instrument suite relevant to current and future missions on Mars. This determination is a critical first step to constrain the formation mechanisms of possible pedogenic deposits on Mars.

1.3. Terrestrial analogs as a window into surface weathering on Mars

In this study, we examined early Oligocene (33 Ma) paleosol profiles from the Mars-analog paleosol sequence in eastern Oregon (Fig. 2).

These samples were analyzed with a suite of instruments that are similar to those used to explore the ancient, altered surface of Mars. Orbital and in-situ visible-near infrared (VNIR) spectroscopic techniques, used by current and future missions to Mars, are a useful tool for identifying alteration minerals and diagenetic features across the global Martian surface (Murchie et al., 2007; Horgan et al., 2017b; Barrington et al., 2020). Here, VNIR spectroscopy was performed to identify clay minerals, zeolites and oxides in bulk paleosol samples. The *Curiosity* Mars rover employs in-situ X-ray diffraction (XRD) for identification and quantification of crystalline minerals in rocks, sediments and soils on Mars (Morris et al., 2016; Rampe et al., 2020). Semi-quantitative XRD was used in this study to identify crystalline minerals in bulk paleosol samples from the three consecutive paleosol profiles. Lastly, samples were analyzed with an instrument calibrated to use analytical conditions similar to the Sample Analysis at Mars evolved gas analysis (SAM-EGA) instrument onboard the *Curiosity* rover (Mahaffy et al., 2012). The purpose of this analysis was to constrain the mineralogy of alteration phases in samples, specifically by examining evolutions of H₂O and SO₂ from bulk paleosol samples during heating. Since thermal techniques such as evolved gas analysis will fly onboard future missions to Mars (e.g. ExoMars 2022 *Rosalind Franklin* rover (Goemann et al., 2017), a detailed characterization of terrestrial paleosol mineralogy with evolved gas analysis can help constrain the formation mechanism(s) of dioctahedral clay-bearing sedimentary rocks on Mars.

2. Methods

2.1. Sample collection

The paleosols examined in this study were collected from the Middle Big Basin Member of the John Day Formation (Fig. 2) near the Painted Hills Unit of the John Day Fossil Beds National Monument in eastern Oregon, USA. For this work, we reoccupied paleosol profiles first described and sampled by Retallack et al. (2000). New samples from three individual paleosols in vertical succession were collected approximately 7 km SW of the entrance to the Painted Hills unit of the John Day Formation (44.631105, -120.213107), in the Middle Big Basin Member of the John Day Formation, approximately 6 m above the local Eocene-Oligocene boundary (Fig. 2). Samples were chosen from this site because it contained a sequence of three successive paleosols at a general topographic position (e.g., badland toeslope) that may be accessible for in-situ analysis on Mars by future landed missions including rovers and/or astronauts. Furthermore, previous ⁴⁰Ar/³⁹Ar dating of volcanic tuffs above and below the sampling location allowed for a constrained age of 33.0 ± 0.10 to 32.7 ± 0.03 Ma (Biotite Tuff and Overlook Tuff, respectively) (Bestland, 1997).

Samples were collected by first trenching to ~30 cm into the outcrop to remove the modern weathering zone and to expose the underlying claystone paleosols. This was followed by sampling with a rock hammer down a vertical transect (parallel with the hillslope) at approximately 10 cm intervals, similar to sampling the horizons of a modern soil profile. Large, ~0.2 kg lithified blocks were removed from the brick-like paleosol surface for mineralogical analyses. The morphology, Munsell color and qualitative calcareousness of samples were also described during collection (Fig. 3).

The three paleosols sampled were a red Alfisol (“Luca” pedotype from (Retallack et al., 2000), a tan Entisol (“Kskus” pedotype), and a brown Inceptisol (“Ticam” pedotype). In modern soil taxonomy, Alfisols are moderately weathered soils typically forming in semi-arid to humid climates under broadleaf temperate forests and are characterized by a clay-enriched subsurface horizon (layer) as well as accumulations of Al and Fe, lending the “Alf” of Alfisol. Entisols are minimally developed soils which are characterized by a lack of pedogenic horizon development and are generally minimally altered from their parent material. Inceptisols are “new soils” and typically have only weak develop-

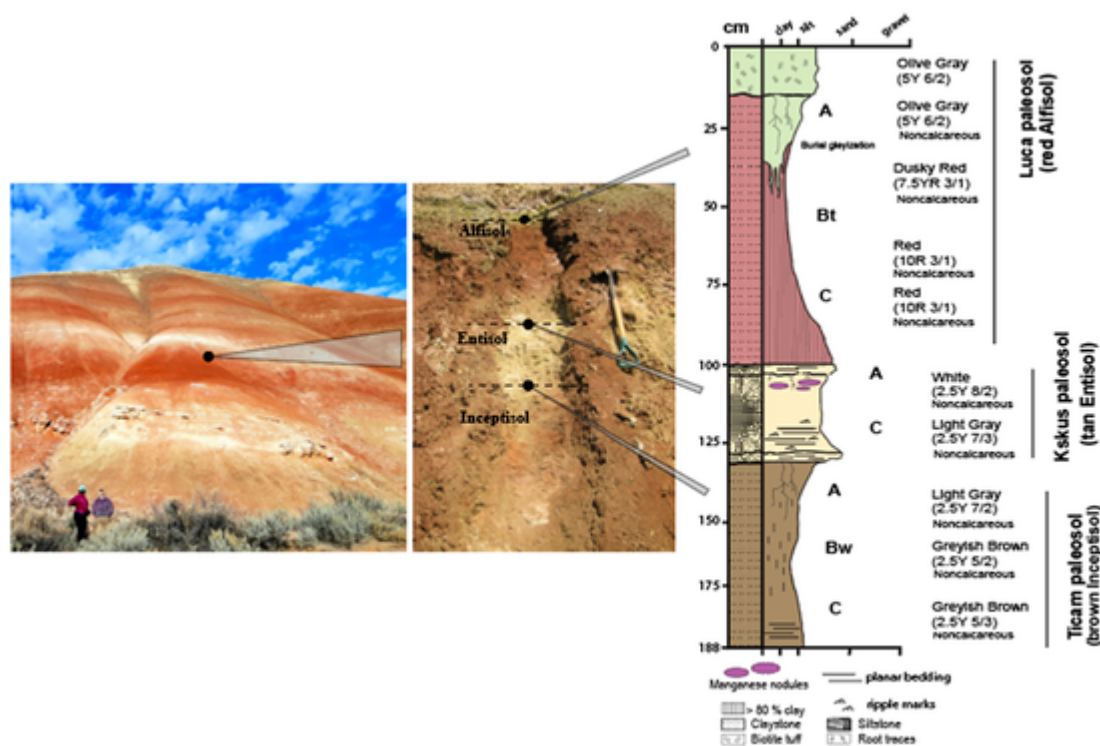


Fig. 3. Morphology of three successive paleosols examined in this work. Paleosols are from the early Oligocene (33 Ma) middle Big Basin Member of the John Day Formation in eastern Oregon, USA showing lithology, grain size, horizon designations, and Munsell color. The upper paleosol (red with drab green top) is a moderately weathered Alfisol (Hapludalf in US Taxonomy (Soil Survey Staff, 2014) with a clay-enriched subsurface (Bt) horizon; stratigraphically below is a minimally weathered and weakly developed Entisol with minimal pedogenic horizon development and persistent relict bedding in the subsurface (C) horizon (Fluvent in US Taxonomy, tan color); the lowest soil (brown color) is an Inceptisol with slight enrichment of clay into a weakly-developed subsurface (Bw) horizon containing relict shards of volcanic glass (Andic Eutrochrept in US Taxonomy). (For interpretation of the references to color in this figure legend, the reader is referred to the web version of this article.)

ment of horizons produced by top-down pedogenic weathering (Soil Survey Staff, 2014).

2.2. Visible-near infrared spectroscopy

Reflectance spectra of paleosols were measured on hand samples collected from the outcrop using a portable ASD QualitySpec Trek spectrometer (Analytik, Cambridge, UK). Reflectance features from 0.35–2.5 μm of samples were measured indoors at ambient (25 °C) temperature at the Condon Paleontology Center at the John Day Fossil Beds National Monument. Samples were not ground or sieved before analysis. Dioctahedral clay mineralogy was inferred from cation-OH combination bands in the 2.2–2.5 μm region (Bishop et al., 2008b). Band centers between 2.12 and 2.21 μm indicated the presence of Al-smectite. Fe/Mg clays and carbonates were identified from absorption bands between 2.27 and 2.36 μm . Oxides were identified from bands between 0.75 and 1.03 μm . Absorption bands from zeolites were considered across the 2.1–2.5- μm range. These overlap with Si-OH and/or metal-OH absorption bands in many phyllosilicates. Zeolites were identified by the presence of absorption bands at 1.9, 1.4 and \sim 1.75 μm . Spectra were not gathered from the thinnest and least developed paleosol (Entisol), but all three paleosol types were subject to X-ray diffraction and evolved gas analysis, discussed below.

2.3. X-ray diffraction of paleosol samples

Paleosols were powdered and homogenized to $< 45 \mu\text{m}$ grain size, then unoriented samples were mounted on aluminum holders and measured using a PANalytical X'pert Pro MPD XRD at NASA Johnson Space Center. XRD patterns were collected using an X'celerator detector and

Co K α X-ray source with a Fe filter to reduce K β peak intensities. Samples were analyzed under the following conditions: 45 kV, 40 mA, $\frac{1}{2}^\circ$ antiscatter slit, $\frac{1}{4}^\circ$ fixed divergence slit, and a beam knife to reduce low-angle scattering. Samples were measured from 4° to $80^\circ 2\theta$ with a 0.02° step size at 100 s/step. Mineral identification was accomplished using HighScore and Jade MDI software by comparing XRD patterns to International Center for Diffraction Data (ICDD) database patterns, and with Crystallography Open Database (COD) patterns.

Semi-quantitative XRD (no internal standard) was used to provide a relative estimate of phyllosilicate abundances. Rietveld refinement (Jones et al., 2000) was carried out using MDI Jade Software with initial structure parameters for crystalline phases from the RRUFF database (<http://rruff.info/>). Background patterns were fit by a polynomial and peaks were modeled by a pseudo-Voigt profile function. Pattern overlays of standard phyllosilicates with known relative intensity ratio (RIR) and full width at half maximum (FWHM) from the Clay Minerals Society (Chipera and Bish, 2001) were used in Rietveld refinements to estimate abundances and types of phyllosilicates in bulk samples. Since no internal standard was used, semi-quantitative XRD was used only for estimating the relative abundances of phyllosilicates in each sample (Table S4).

2.4. Thermal and evolved gas analysis (EGA) of paleosol samples

A Setaram Labsys Evo differential scanning calorimeter (DSC) / thermal gravimeter (TG) connected to a Pfeiffer Omnistar quadrupole mass spectrometer (QMS) was configured to operate similarly to the SAM evolved gas analyzer. The Sample Analysis at Mars (SAM) onboard Curiosity Mars Rover does not have TG/DSC capabilities, but these components permit a better understanding of phase transitions and chemical reactions in laboratory experiments. Approximately $50 \text{ mg} \pm 3 \text{ mg}$

of ground paleosol sample were placed in a clean Al_2O_3 crucible. Prior to use, the crucible was ashed at 500°C to remove organic contaminants. The sample crucible and an identical empty reference crucible were placed in the furnace and then the system was purged twice with helium gas and then set to a pressure of 30 mbar. Helium was chosen as a carrier gas because it is inert and because it used as a carrier gas in the SAM instrument. The crucibles were heated from approximately 35°C to 1000°C at a heating rate of $35^\circ\text{C}/\text{min}$ and at a flow rate of 10 sccm. Volatiles ranging from mass/charge (m/z) 1–100 were measured. All analyses were performed in duplicate.

Evolved water abundances were determined using a Netzsch TG/DSC coupled to a Pfeiffer QMS. An Al_2O_3 sample crucible and an identical reference crucible were placed in the furnace. The instrument was purged twice with ultra-high purity O_2 and set to a pressure of 1000 mbar prior to sample analyses to remove any contamination in the system. The crucibles were heated from approximately 35°C to 1000°C at a heating rate of $35^\circ\text{C}/\text{min}$ and at a flow rate of 19 ml O_2/min . A series of three blanks were analyzed before and after each group ($n = 10$) of samples. A calibration curve for CO_2 was created by analyzing a calcite standard (Iceland sparry calcite $40\ \mu\text{M}$) at eight sample masses ranging from 0.01–4 mg. This calibration curve was used to calculate the amount of CO_2 evolved from each sample, and these values were converted to weight percent and subtracted from the thermogravimetric data to estimate mass loss from water evolutions. Oxygen was chosen as a carrier gas because it encourages complete combustion of all organic and inorganic carbon in samples, which indirectly allowed for calculation of evolved water abundances. Since there were no major overlapping gases with evolved water, mass loss from low amounts ($< 0.1\ \text{wt}\%$) of organic and inorganic carbon were the only significant sources of mass loss aside from water loss from hydrated phases ($\sim 3\text{--}5\ \text{wt}\%$). The remaining mass loss after accounting for CO_2 evolutions was attributed to evolved H_2O , thus allowing for estimates of evolved water abundances from the thermogravimetric data. All analyses were performed in duplicate.

2.5. Bulk geochemistry and grain size

We used previously published estimates of paleosol bulk geochemistry and grain size to provide a reference frame for interpreting the mineralogy and diagenesis of samples examined in the present study (Retallack et al., 2000; Sheldon et al., 2002). The same paleosol profiles examined in this work were previously analyzed for bulk geochemistry and grain size by Retallack et al. (2000) and those previously published values were used to augment our new mineralogical assessment of the same samples (see Results).

Retallack et al. (2000) collected oriented paleosol samples for point counting and bulk geochemistry. They performed point counting (500 points) to determine relative percent of sand, silt and clay size fractions using a Swift automated stage and Hacker counting box fitted to a Leitz Orthoplan Pol research microscope. Major element chemistry of paleosols, also previously performed by Retallack et al. (2000), was determined by X-ray fluorescence and atomic absorbance spectroscopy at Washington State University, Pullman (Table S1). These previously published data were used to calculate chemical index of alteration (CIA) of each paleosol profile examined in this work. Major element chemistry and molar weathering ratios from Retallack et al. (2000) are included as supplementary data (Table S1).

3. Results and discussion

3.1. Chemical weathering trends

As originally noted in Retallack et al. (2000) and Sheldon et al. (2002), trends in molecular weathering ratios and chemical index of alteration across the three paleosol types were attributed to differences in chemical weathering intensity and duration. All profiles showed evidence of hydrolysis of volcanoclastic sediments from increases in alumina/silica and alumina/bases toward the top of profiles (Fig. 4). The clay size fraction ranged from 75.0 to $95.4 \pm 2\ \text{wt}\%$ and was greatest in the subsurface (Bt) horizon of the Alfisol and lowest in the surface

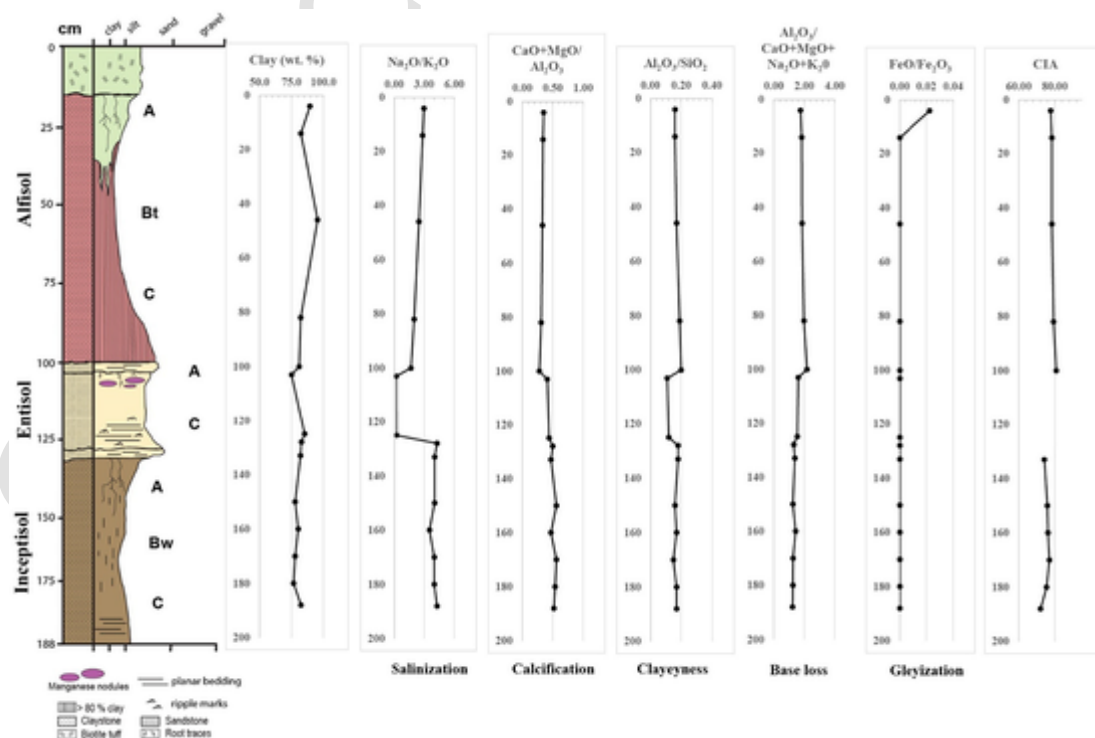


Fig. 4. Chemical weathering trends as a function of depth across three paleosol profiles from the Oligocene (33 Ma) Big Basin Member of the John Day Formation (Data from Retallack et al. (2000)). CIA = Chemical index of alteration, not shown for the weakly developed Entisol (middle profile).

(A) horizon of the Entisol. Generally low ranges of calcification ($\text{CaO} + \text{MgO}/\text{Al}_2\text{O}_3$) were noted in all three profiles and suggested minimal or absent accumulation of CaCO_3 . This is characteristic of subtropical to temperate soils receiving annual rainfall of 600–1200 mm (Sheldon et al., 2002). Pedogenic CaCO_3 typically accumulates in arid to semi-arid soils where annual evapotranspiration exceeds precipitation (Breecker et al., 2009) and thus significant CaCO_3 accumulation was unlikely for paleosols from the Big Basin Member of the John Day Formation. There were negligible trends in alumina/silica ratios, but declining trends in $\text{Na}_2\text{O}/\text{K}_2\text{O}$ suggest slight salinization in the uppermost paleosol (Alfisol), although this trend terminated in the surface (A) horizon of the Inceptisol. Salinization, a rough measure of the original salt content of paleosols, is defined by the molar ratio of Na_2O to K_2O and results from the deposition and/or precipitation of salts in the original soil. Minimal salinization may have caused the slight increase in this ratio at the surface of the Alfisol, but salinization was likely not severe because there was a lack of domed columnar peds and salt crystals that are characteristic of salt-affected soils and paleosols (Retallack et al., 2018; Retallack, 2019). Lack of carbonate and generally deep weathering inferred from high smectite content is consistent with acidic pH, but low alumina/bases ratio, smectite mineralogy and residual feldspar clasts indicate moderate base saturation across all profiles. A pH of ~5.5–7.5 is characteristic of Alfisols formed in similar climates (Retallack et al., 2000), but diagenetic fluids can alter the original soil pH after burial and lithification, thereby obscuring primary pH values (Lukens et al., 2018). High oxidation of iron ($\text{FeO}/\text{Fe}_2\text{O}_3 = 0$) and deeply penetrating root traces indicate soil formation in well-drained settings. However, the surface (A) horizon of the Alfisol showed slight gleyization ($\text{FeO}/\text{Fe}_2\text{O}_3 > 0$) most likely from the onset of chemically reducing conditions shortly after burial. This has been attributed to a diagenetic phenomenon known as burial gleization (discussed in detail in Section 3.5) that typically affects the organic matter-rich surface horizons of rapidly buried paleosols (Retallack, 1991).

The chemical index of alteration (CIA) ranged from 72.1 to 80.8 and generally decreased with depth across the Alfisol and Inceptisol (Fig. 4). The highest values (80.8) were in the subsurface clay (Bt) horizon of the Alfisol and lowest (72.1) in the C-horizon of the Inceptisol. The CIA in clayey paleosols is generally highest in subsurface horizons due to illuvial accumulation of clay minerals during top-down hydrolytic weathering, and therefore subsurface (B) horizons are thought to be the most reliable for paleoclimate estimations (Sheldon et al., 2002). In contrast, the unweathered lowermost C and R horizons of paleosols (e.g., saprolite) reflect the characteristics of the soil parent material rather than alteration from weathering, and thus CIA is lower in these horizons. The thinnest and least developed paleosol (Entisol) preserved a parent material of redeposited tuffaceous clayey siltstone that was minimally altered by soil formation, inferred from relict bedding in the C-horizon. The high clay content of this paleosol (~75 wt%) was most likely inherited from preexisting soils by sheet erosion or flooding (Retallack et al., 2000). It is unlikely that the Entisol was developed for long enough to develop characteristics indicative of paleoclimate, and therefore estimations of CIA are unreliable and not shown.

3.2. Visible/near infrared (VNIR) spectroscopy of paleosols

The mineralogy of paleosols as observed with VNIR spectroscopy was dominated by dioctahedral phyllosilicates and occasionally zeolites and hematite. All paleosol samples had strong spectral signatures of 2:1 Al/Fe dioctahedral smectites (Fig. 5). Distinct changes in mineralogy were observed within and between paleosol profiles. Spectral absorption bands were consistent with mixtures of Al-montmorillonite and Fe-nontronite, and/or Fe substitution in montmorillonite. There were no apparent reflectance features characteristic of trioctahedral smectites such as saponite (Chemtob et al., 2015) or 1:1 smectites such as kaolin group clays (Bishop et al., 2008b).

At the stratigraphically highest location, the near-surface horizon of the Alfisol, characterized by a drab green color, showed strong spectral signatures of Al-smectite with an asymmetric doublet feature centered at 2.22 μm with shoulders at 2.21 and 2.25 μm , and a strong water band at 1.92 μm (Figs. 5 and 6). Band depths of the 1.9 and 2.2 μm absorption bands were variable across all samples (Supplementary Data). Al smectites such as montmorillonite have a characteristic band at 2.21 μm , but the position of this band varies with Al-Fe-Mg abundance, where substitution of Fe for Al can cause additional bands at 2.23–2.25 μm (Bishop et al., 2008b). A broad absorption band beginning near 2.4 μm was consistent with zeolites such as clinoptilolite. Zeolites are likely also responsible for the strong hydration overtone bands at 0.98, 1.19, 1.45, 1.78, and 1.95 μm , of which usually only the 1.4 and 1.9 μm bands are visible in most other hydrated minerals. Diagenetic zeolitization of a poorly crystalline smectite or volcanic glass is thought to have led to the formation of clinoptilolite in paleosols from the John Day Formation (Retallack et al., 2000). At shorter wavelengths, the sample showed a shoulder at 0.5 μm and a strong band at 0.65 μm due to Fe^{3+} in smectite, as well as a broad weak absorption near 1.1 μm likely due to $\text{Fe}^{2+}/\text{Fe}^{3+}$ in smectite (Bishop et al., 2008b).

Stratigraphically lower, the subsurface (Bt) horizon of the Alfisol had much weaker signatures of an Al smectite with minor amounts of Fe-smectite (Fig. 5). Below this sample, the Alfisol C-horizon had a broad absorption band at 0.9 μm attributed to hematite, as well as weak absorption bands of Al smectite similar to the Bt-horizon. The 0.65 and 0.95 μm bands were absent in these samples which was consistent with an absence of Fe-smectite. Hematite in the C-horizon of the Alfisol may have formed from burial dehydration of ferric (oxy)hydroxides (e.g., goethite) which is a common diagenetic alteration in paleosols (Retallack, 2019). Bulk geochemistry of the Alfisol samples indicated lower Fe_2O_3 in the surface horizons of samples relative to subsurface horizons (Table S1) which is consistent with VNIR detections of hematite in subsurface horizons.

All samples of the brown colored Inceptisol had spectral signatures of a mixed Al/Fe smectite, with a clear band centered at 2.21 μm , a shoulder at 2.23 μm , and a weak band at 2.29 μm , and no detection of hematite. Strong absorption bands near 1.45 and 1.91 μm and a shoulder at 2.23 μm were consistent with Opal-CT (Yant et al., 2018). The light brown Munsell color of this sample (2.5Y 5/2) was markedly different than the brick-red (10R 7/1) color of the overlying Alfisol and suggests hematite abundances were much lower or absent in the Inceptisol. Sharp 0.65 and 0.95 μm Fe smectite absorption bands throughout the profile were consistent with accumulations of nontronite and/or Fe montmorillonite. Like the overlying Alfisol, band depths of the 1.9 and 2.21 μm absorption bands were also variable across all samples in the Inceptisol profile (Table S1).

The spectral “doublet” feature with bands near 2.21 and 2.23–2.25 μm was observed in all samples and was attributed to OH stretching and bending combination vibrations in phyllosilicates (Fig. 6). Doublet-type spectra typically represent mixtures of various hydrated minerals including kaolinite, Al-smectites and sulfate minerals (Danielson et al., 2019; Bishop et al., 2020). Previous work has shown that $\text{Fe}^{2+}/\text{Fe}^{3+}$ smectites exhibit bands in this region (Chemtob et al., 2015). A doublet feature near 2.21 and 2.23–2.25 μm may be a unique spectroscopic feature of pedogenic smectites that results from isomorphous substitution of Al in the tetrahedral layer of 2:1 phyllosilicates during subaerial weathering (Horgan et al., 2017c). Previous work on smectite-rich mafic soils and paleosols show similar doublet features between 2.2 and 2.3 μm that are absent in standard clays (Bishop et al., 2008b; Horgan et al., 2011). The position and shape of the bands tends to be highly variable (Horgan et al., 2017c). These doublet features noted in paleosol samples here are similar to doublet features previously observed in other paleosols from the John Day Formation (Horgan et al., 2011). Thus, the doublet features here are consistent with a pedogenic origin for Fe/Al smectites, as has been previously sug-

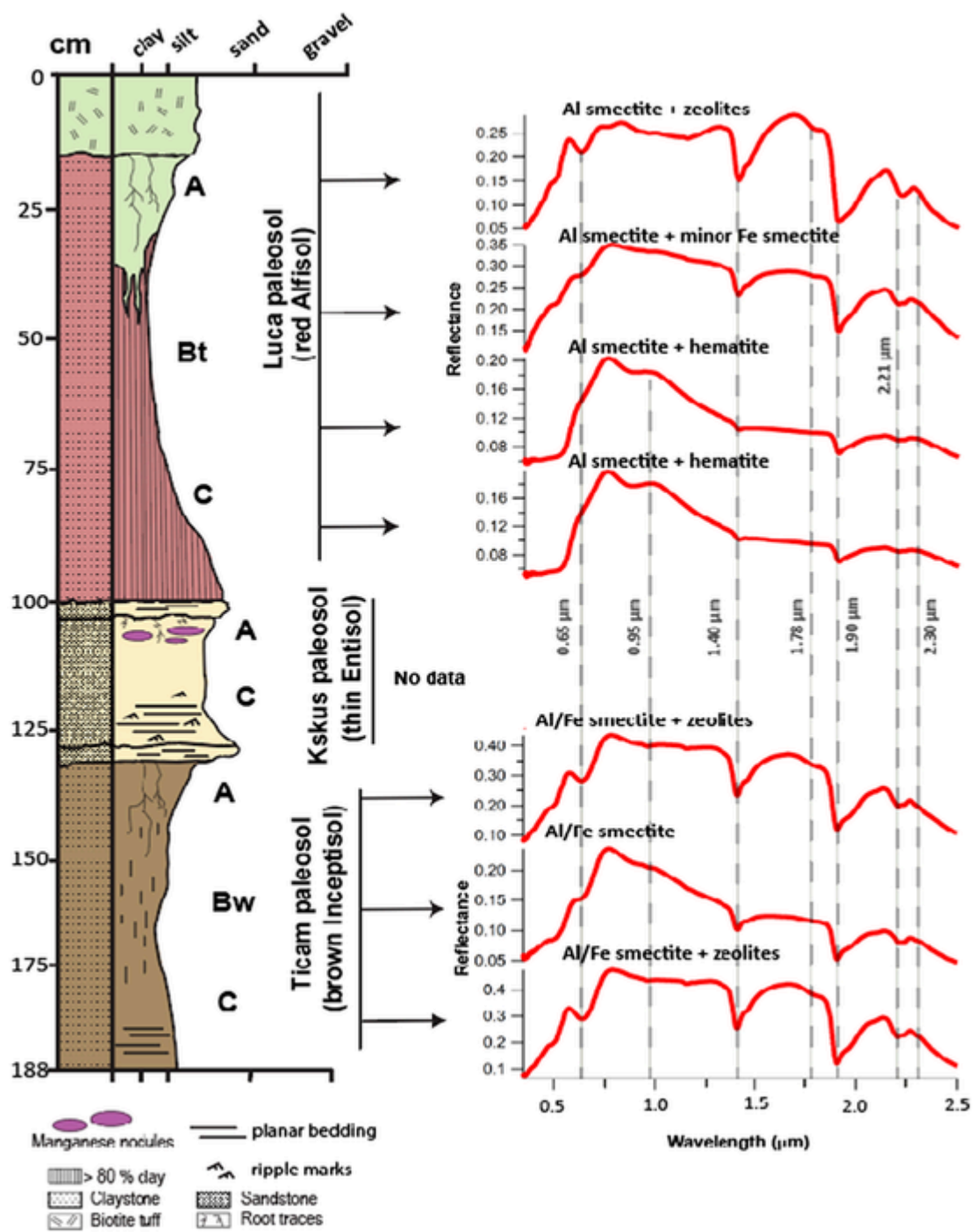


Fig. 5. Visible/near infrared reflectance (VNIR) spectra of two paleosols (Alfisol and Inceptisol) from the early Oligocene (33 Ma) middle Big Basin Member of the John Day Formation in eastern Oregon, USA. Vertical dotted lines at 0.65, 0.95, 1.4, 1.78, 1.90, 2.21, and 2.30 μm represent absorption features characteristic of Al and/or Fe smectite, hematite and/or zeolites.

gested. However, it should be noted that the doublet feature has not been observed in modern silicic soils, (Horgan et al., 2017a, 2017c), so absence of the feature is not necessary evidence against a pedogenic origin for clay minerals.

3.3. X-ray diffraction of paleosols

XRD diffractograms showed strongly crystalline clay minerals dominated all samples (Fig. 7, Table 1). Major phases identified in all samples (> 5 wt%) were montmorillonite (Al smectite) and nontronite (Fe smectite) while minor phases (< 5 wt%) identified from patterns in all

samples were clinoptilolite, cristobalite, Opal-CT, quartz, andesine, orthoclase, gypsum and jarosite. Montmorillonite and nontronite were identified as distinct phases using Rietveld refinements (see Methods). Notably, the zeolite mineral clinoptilolite ($\text{Na}_{.66}\text{Ca}_{.86}\text{K}_{.64}\text{Mg}_{.26}\text{Si}_{18}\text{O}_{49.42}\text{H}_{26.4}$) was identified from patterns in all paleosol samples, which likely formed from post-burial alteration of volcanic glass or other poorly ordered phases including smectite during Miocene-age burial recrystallization (Retallack et al., 2000).

Beginning with the stratigraphically highest sample (Alfisol 4 cm), major phases identified from patterns were montmorillonite and nontronite while minor phases identified were andesine, Opal-CT and

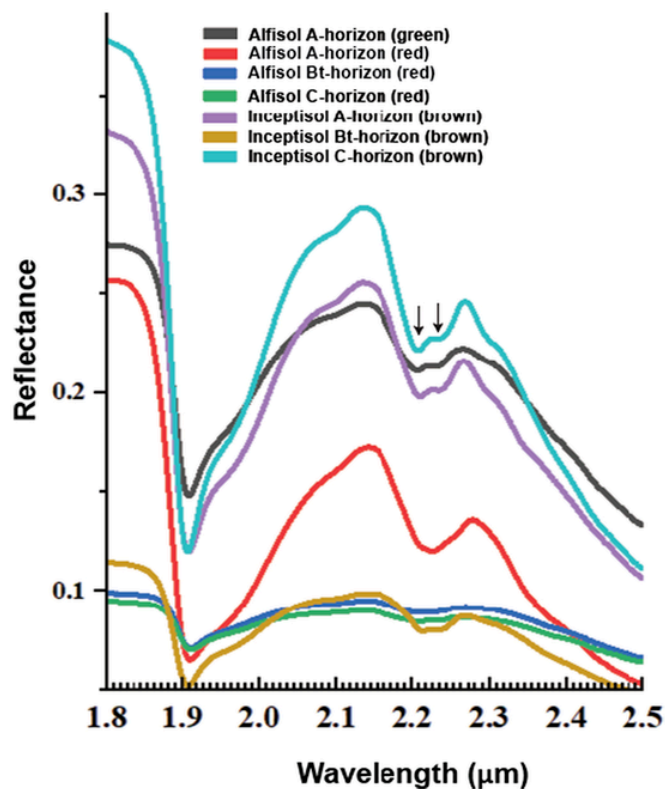


Fig. 6. Near-infrared spectra from surface and subsurface horizons of two paleosols (Alfisol and Inceptisol) from the early Oligocene (33 Ma) middle Big Basin Member of the John Day Formation. Spectral doublet feature between 2.2 and 2.23–2.25 μm is indicated with black arrows.

cristobalite, with lesser abundances of clinoptilolite, quartz, gypsum, jarosite, and anatase (Fig. 7). Stratigraphically below this sample, the Alfisol A-horizon at 14 cm showed a similar mineral assemblage with the addition of albite as a minor phase (Table 1). A deeper sample of the Alfisol at 46 cm (Bt horizon) had montmorillonite and nontronite as major phases and albite, cristobalite, opal-CT, clinoptilolite, hematite,

quartz and anatase as minor phases. Directly below, the pattern from Entisol A-horizon at 7 cm was consistent with montmorillonite and nontronite as major phases and cristobalite, anatase, clinoptilolite, and orthoclase as minor phases (Fig. 7). Stratigraphically below this sample, the pattern for the near-surface (A) horizon of the Inceptisol (3 cm) showed montmorillonite, nontronite and Opal-CT as major phases and clinoptilolite, cristobalite, andesine, orthoclase, quartz, and gypsum as minor phases. The pattern from the stratigraphically lowest sample, the Inceptisol Bw-horizon at 21 cm, showed the same major phases as the A-horizon (3 cm) sample, but with the additions of hematite, ilmenite (FeTiO_3) and anatase along with clinoptilolite, cristobalite, quartz and andesine as minor phases.

The abundance of crystalline clay minerals across all samples is consistent with pedogenic surface weathering of andesitic to rhyolitic tuff / ash under a temperate climate (MAT of $\sim 10^\circ\text{C}$ and MAP of 600–1200 mm) over 10–100 Kyr of soil formation (Retallack et al., 2000). This agrees with other estimates of MAT $> 12^\circ\text{C}$ and MAP of > 1000 mm from geochemical climofunctions applied to the subsurface horizons of paleosols from the middle Big Basin Member (~ 33.7 Ma) of the John Day Formation (Sheldon et al., 2002). This amount of surface weathering over tens to hundreds of thousands of years transformed most volcanic glass to smectite via hydrolytic weathering, potentially leaving only a small x-ray amorphous component (e.g., unweathered volcanic glass and/or poorly ordered phases) which presumably was diagenetically altered via zeolitization to clinoptilolite. There were no XRD detections of illite which suggests minimal or absent potash metasomatism despite burial by an estimated ~ 2 km of overburden (Novoselov et al., 2015).

3.4. Evolved gas analysis

3.4.1. H_2O evolutions

All samples evolved H_2O (m/z 18) during evolved gas analyses. This was attributed to the release of adsorbed water, interlayer water, and water from dehydroxylation in the octahedral layer of a dioctahedral clay mineral (Fig. 8). Low temperature ($< 450^\circ\text{C}$) and high temperature ($> 450^\circ\text{C}$) evolutions of water from paleosol samples co-occurred with an endotherm in the heat flow data (dotted line, Fig. 8) resulting from endothermic dehydration and dehydroxylation reactions, respec-

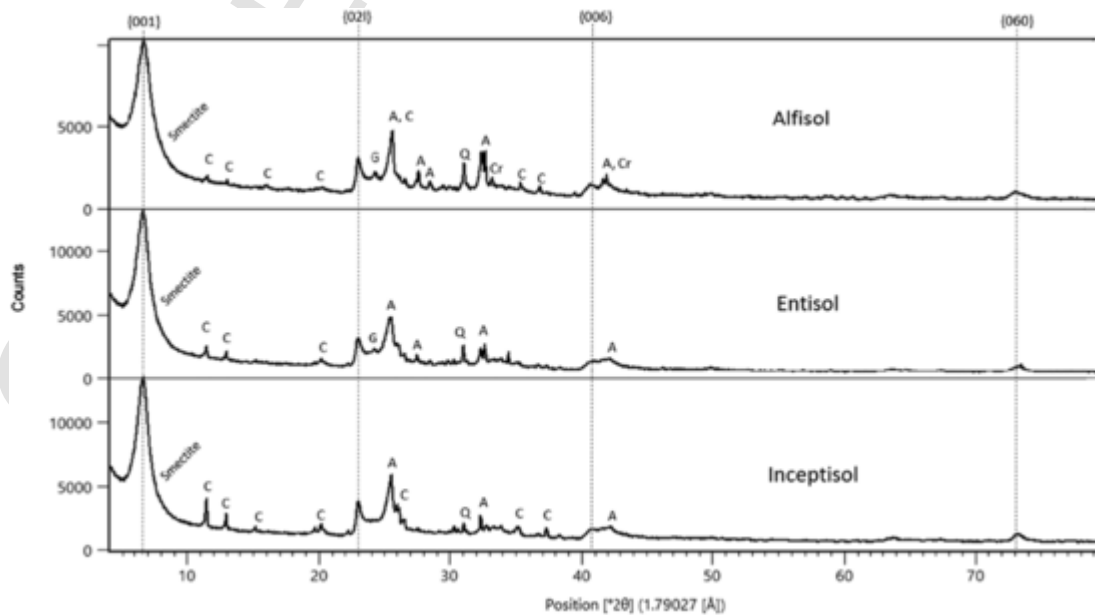


Fig. 7. X-ray diffraction patterns from the near surface (A-horizon) of three paleosols from the early Oligocene (33 Ma) middle Big Basin Member of the John Day Formation in eastern Oregon, USA. S = Smectite; G = Gypsum; A = Andesine; C = Clinoptilolite; Cr = Cristobalite; Q = Quartz. Highlighted are the 001 and 021 smectite peaks; difference in 021 band position corresponds to a difference in octahedral occupancy.

Table 1

Summary of major and minor phases detected with x-ray diffraction. Major phases (> 5 wt% are noted with an X while minor phases (< 5 wt%) are noted with an asterisk.

	Alfisol (4 cm)	Alfisol (14 cm)	Alfisol (46 cm)	Entisol (3 cm)	Entisol (7 cm)	Inceptisol (3 cm)	Inceptisol (7 cm)
Montmorillonite	X	X	X	X	X	X	X
Nontronite	X	X	X	X	X	X	X
Saponite			*				
Andesite		X				*	*
Clinoptililite		*		*	*	*	*
Cristobalite	*	*	*	*	*	*	*
Opal-CT	*	*	*	X	X	X	X
Quartz	*	*	*	*	*	*	*
Anatase	*	*	*	*	*	*	*
Albite		X	X	*			
Orthoclase					*	*	*
Hematite			*				*
Gypsum	*		*	*	*	*	*
Jarosite	*						
Others/Amorphous				*	*	*	*

tively. Evolved water abundances ranged from 3.24 ± 0.47 wt% to 5.03 ± 0.12 wt% H₂O across all samples ($n = 20$) and trends in water abundances were apparent across the three paleosols. The Alfisol evolved the lowest amount of water observed with 3.24 ± 0.47 in the subsurface (Bt) horizon whereas the Entisol averaged 5.03 ± 0.12 wt% which was the highest amount of evolved water observed in the experiment. The Inceptisol ranged from 4.32 ± 0.03 wt% to 4.81 ± 0.13 wt% H₂O and showed a trend of decreasing abundance with depth. Despite significant differences in evolved water abundances between profiles, each profile generally showed a decrease in evolved water abundance with depth. Though many factors control the abundance and persistence of hydrated phases in paleosols, trends in evolved water abundances could have resulted from lateral and vertical diversity in mineralogy within each of the profiles.

Water evolutions at temperatures less than 300 °C were consistent with adsorbed water on mineral surfaces (Earnest, 1991). Evolutions of H₂O between 100 °C and 300 °C can result from the release of interlayer H₂O from smectite and other 2:1 clay minerals (McAdam et al., 2020) or from dehydroxylation and/or dehydration of poorly crystalline, nanophase or amorphous aluminosilicates such as allophane and imogolite (Smith et al., 2018b). Nanophase oxides/oxyhydroxides including ferrihydrite can evolve adsorbed H₂O at temperatures ranges below ~450 °C due to their high specific surface areas (Sutter et al., 2017) and could have contributed to water evolutions below 200 °C. Other sources of minor H₂O evolutions near 300 °C were consistent with oxyhydroxides such as goethite which dehydroxylate at temperatures ranging from 280 to 320 °C (Sutter et al., 2008).

Differences in evolved H₂O peaks < 450 °C across the three paleosols examined here may have resulted from differences in abundance and composition of x-ray amorphous components. Though amorphous phase composition was not examined in this work, a previous study identified basaltic glass (5.6 wt%), allophanes (7.9 wt%) and ferrihydrite (0.6 wt%) as the dominant amorphous phases in paleosols from the Oligocene (~28 Ma) Turtle Cove member of the John Day Formation (Smith et al., 2018a, 2018b) which are stratigraphically higher than paleosols examined here (Fig. 1). Turtle Cove paleosols have mineralogical and paleobotanical evidence of a cool and dry climate of an estimated MAP of 400–600 mm (Fig. 2) and thus minor alteration of volcanic ash and tuff (Sheldon et al., 2002). A SAM-EGA analog analysis of a Turtle Cove paleosol was performed by Smith et al. (2018a, 2018b) (Smith et al., 2018b) who noted a water release peak at ~290 °C which was attributed to the abundance (> ~40 wt%) of amorphous materials in the sample, unlike the low amount (< 5 wt%) of x-ray amorphous phases found in smectitic paleosols in the middle Big Basin member of the John Day Formation. Paleosols from the Big Basin Member formed under a much warmer (MAT 16–18 °C) and wetter (MAP 600–1200 mm) climate than those from the Turtle Cove Member which

was sufficient to transform amorphous and nanocrystalline phases to Al/Fe smectites. In the present study there were no sharp water release peaks at ~290 °C (Fig. 8), possibly because samples were composed primarily of strongly crystalline clay minerals rather than amorphous colloids (Fig. 3). However, a minor 300 °C endotherm in all samples was consistent with small amounts of amorphous phases. Amorphous and/or nanocrystalline materials were also detected with XRD as minor phases in the Entisol and Inceptisol (Table 1). Differences in the duration of weathering before burial may explain the persistence of amorphous phases in the Entisol and Inceptisol and absence of amorphous phases in the Alfisol. In contrast to the moderately weathered Alfisol, the Entisol and Inceptisol were only minimally weathered before burial, inferred from morphological features such as absence of clay illuviation and persistence of relict bedding in subsurface horizons (Fig. 3).

Overall, the preservation of metastable amorphous phases over geological time scales is uncommon in sedimentary rocks; however, recent work has shown that large amounts (> 40 wt%) of amorphous colloids have persisted for millions of years in lithified and diagenetically altered volcaniclastic paleosols from the Oligocene (~28 Ma) Turtle Cove Member of the John Day Formation (Smith and Horgan, 2021). Thus, detections of minor amounts of amorphous phases (< 5 wt%) with both EGA and XRD suggest metastable amorphous and/or nanocrystalline phases may have also persisted for ~33 Ma in paleosols from the middle Big Basin Member of the John Day Formation.

Evolutions of H₂O above 450 °C are consistent with the dehydroxylation of the octahedral layer of a 2:1 phyllosilicate (Ming et al., 2014; McAdam et al., 2020). There was a ~200 °C difference in H₂O peak release temperature between the three paleosols. Differences in clay mineralogy between the soils may be responsible for shifting the peaks and shoulders of the high-temperature (> 450 °C) evolutions. The Alfisol with ~95 wt% smectite evolved H₂O with peaks centered at ~500 °C, while the Entisol (~75 wt% smectite) and the Inceptisol (~78 wt% smectite) evolved H₂O with peaks centered at ~700 °C. The considerable difference in peak H₂O release temperature between the red Alfisol (~500 °C) and the other soils (~700 °C, Fig. 8) could have resulted from differences in the occupation of the octahedral sheet of a 2:1 phyllosilicate (Earnest, 1991) which leads to differences in the high temperature H₂O peak release temperature during SAM-EGA (Hogancamp et al., 2017; McAdam et al., 2017). Clay minerals with Fe in the octahedral layer (e.g., nontronite or Fe-montmorillonite) dehydroxylate at a lower temperature (~500 °C) relative to smectite with Al in the octahedral layer (e.g., Al-montmorillonite, 700 °C) (McAdam et al., 2017), though mixed illite-smectite mineralogy also show peak H₂O release at ~700 °C (Earnest, 1991; McAdam et al., 2017). The Alfisol (~500 °C peak H₂O release) exhibited strong VNIR signatures of an Al-smectite with minor Fe-smectite and hematite. The brown Inceptisol (~700 °C peak H₂O release) had strong VNIR signatures of an Al/Fe smectite and

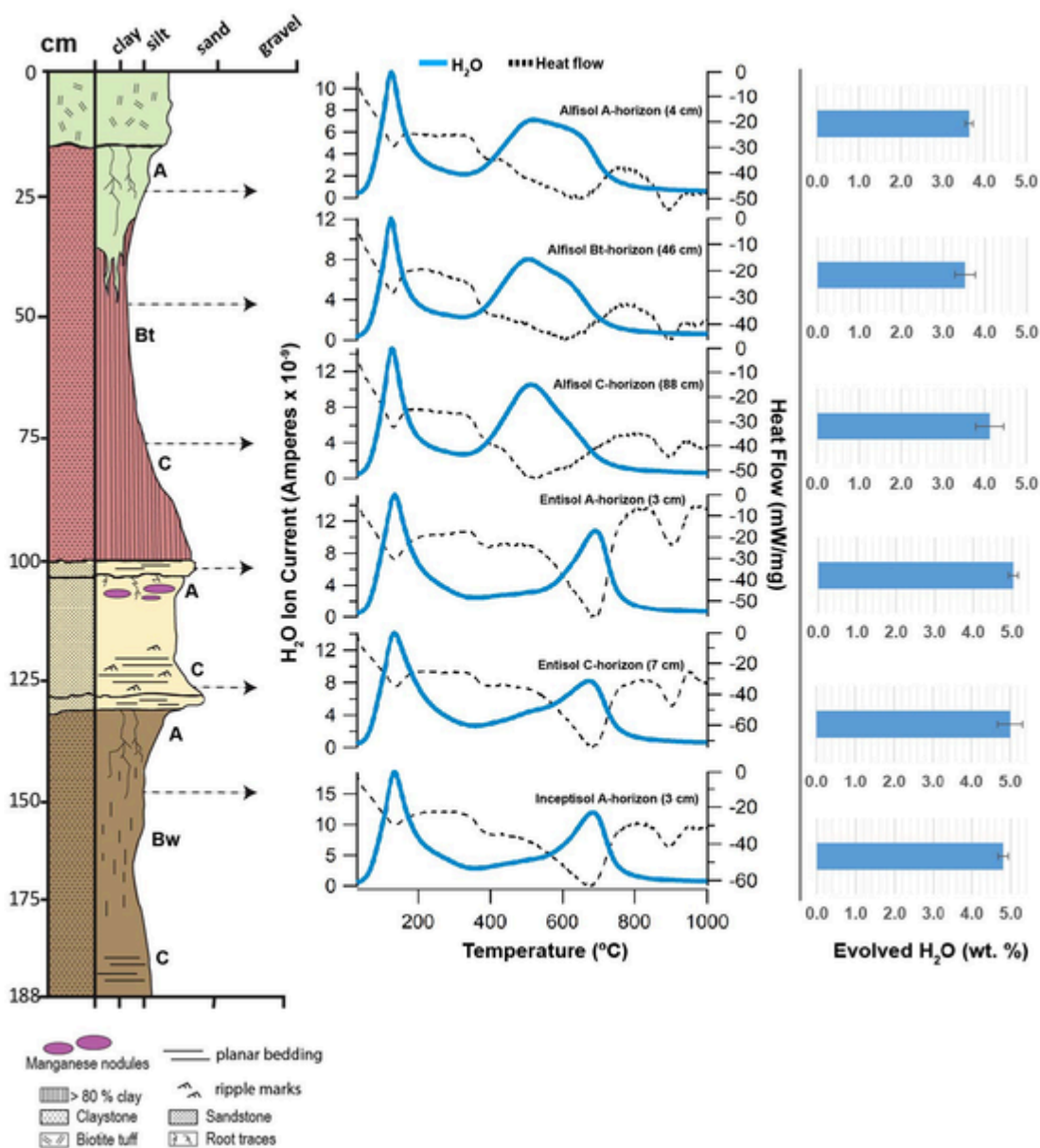


Fig. 8. Evolutions of H₂O from early Oligocene (33 Ma) paleosols from the John Day Fossil Beds National Monument, Oregon. Blue trace is H₂O (*m/z* 18), and dashed trace is heat flow from differential scanning calorimetry (DSC). (For interpretation of the references to color in this figure legend, the reader is referred to the web version of this article.)

lacked hematite (Fig. 5). Differences in Fe content of the smectites likely caused the large difference (~200 °C) of peak water release temperatures from smectite dehydroxylation. Together these results suggest that EGA in conjunction with XRD and VNIR spectroscopy are suitable techniques to constrain smectite mineralogy in paleosols.

3.4.2. SO₂ evolutions

All samples evolved minor amounts of SO₂ primarily above 450 °C (Fig. 9). Minor SO₂ peaks below 400 °C were observed in the Bt horizon of the Alfisol and the A-horizon of the Entisol (Fig. 9) which most likely resulted from instrument background sources. A distinct SO₂ peak at 400 °C in the A-horizon of the Entisol is consistent with the presence of minor amounts of sulfides such as pyrite and/or pyrrhotite which thermally decompose at temperatures above 400 °C under SAM-EGA analog conditions (McAdam et al., 2014). Oxidative sulfite decomposition directly to SO₂ could have resulted from trace amounts of oxygen in the instrument furnace even after successive purges with helium and are the likely source of the broad 400 °C SO₂ peak noted in the Entisol.

Evolutions of SO₂ above 500 °C are consistent with the thermal decomposition of Ca and Fe sulfates ranging from crystalline (gypsum and jarosite) to amorphous and/or adsorbed sulfate (McAdam et al., 2014; Sutter et al., 2017). Also possible are contributions from organo-sulfur compounds and/or S phase inclusions in volcanic glass. Crystalline sulfate species including jarosite and gypsum have peak SO₂ release temperatures near 900 °C and 1200 °C, respectively (Sutter et al., 2008). Thus, jarosite and gypsum most likely account for the evolutions of SO₂ above 600 °C and both were confirmed as minor phases with XRD (Table 1). Samples from the Bt and C horizons of the Alfisol had a broad SO₂ release with a peak at ~790 °C that was absent in the Entisol and Inceptisol. Trace amounts of Mg sulfates in the Alfisol could account for minor SO₂ releases >700 °C including the ~790 °C SO₂ peaks (François et al., 2015; McAdam et al., 2020) At higher temperatures, all soils showed a major release of SO₂ beginning at 900 °C which co-occurred with an endotherm, both of which are consistent with the thermal decomposition of crystalline sulfates (Ming et al., 2014; François et al.,

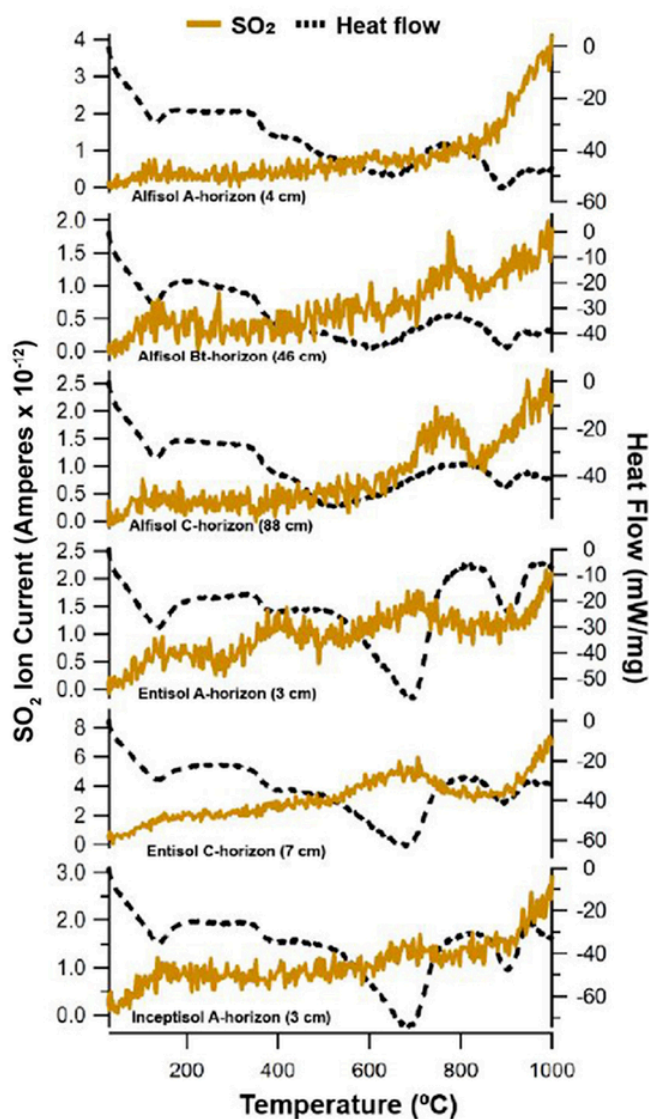


Fig. 9. Evolutions of SO_2 from early Oligocene (33 Ma) paleosols from the John Day Fossil Beds National Monument, Oregon. Yellow trace is SO_2 (m/z 64), and dashed trace is heat flow from differential scanning calorimetry (DSC). (For interpretation of the references to color in this figure legend, the reader is referred to the web version of this article.)

2015). Since the samples were only heated to $\sim 1000^\circ\text{C}$ for this work, the maximum peak height of this release cannot be ascertained.

The presence of sulfate minerals is uncommon in smectite-rich soils such as those examined here. Sulfate minerals such as gypsum and jarosite tend to form at low pH and low water:rock ratios whereas pedogenic smectites such as montmorillonite typically form at circumneutral pH and increased water:rock ratios. Both gypsum and jarosite are unlikely to be original minerals in the paleosols; it is more likely they formed in the current weathering zone. One possibility for the origin of sulfate minerals in these paleosols is leaching from the modern soils forming atop paleosols (e.g., the current weathering zone). These modern soils that mantle paleosol outcrops have visibly accumulated pedogenic gypsum into a thin (~ 1 cm) subsurface gypsic (By) horizon, allowing for their classification as Gypsisols (gypsum-rich desert soils) in US Soil Taxonomy (Soil Survey Staff, 2014). The modern soils are subject to an estimated MAT of 33°C and MAP of 290 mm which is significantly warmer and drier than the estimated conditions during the formation of John Day Formation paleosols (MAT $16\text{--}18^\circ\text{C}$ and MAP of 600–1200 mm). Sulfate minerals observed with XRD and EGA could

have accumulated over time in the underlying paleosols and therefore it is likely that the modern Gypsic soils forming atop paleosol outcrops are the source of sulfate minerals observed here.

3.5. Diagenetic alteration

Diagenetic alterations, or alterations after burial, are common in paleosols. By definition, soils are an early diagenetic alteration because water-rock interactions during pedogenesis alters the physical and chemical properties of sediments. After burial, however, soils are subject to additional early and late diagenetic alterations ranging from minor (e.g., decomposition of organic matter) to severe (e.g., metamorphism to greenschist facies). Four types of alteration after burial that have affected paleosols examined in this work are 1) Drab olive-green surface horizons attributed to burial gleization; 2) brick-red color from burial-induced dehydration of ferric hydroxide minerals; 3) zeolitization of volcanic glass and/or poorly crystalline phases; and 4) significant mechanical compaction.

Burial gleization, also known as gley overprinting (Driese and Ober, 2005), has been envisaged as the chemical reduction of iron oxides and hydroxides by anaerobic bacteria in the near-surface horizons of paleosols and is thought to occur shortly after soil burial (Retallack, 1991; PiPujol and Buurman, 1994). Burial gleization is an early diagenetic process in paleosols which involves the reduction of Fe^{3+} to Fe^{2+} in clays, oxides and other minerals after rapid burial, and promotes anaerobic decay of organic matter (Retallack, 2019), even in soils that originally formed under oxidizing conditions before burial. Typical burial gleization is closed system alteration, without depletion of total iron, and is usually limited to the surface (A) horizons where organic matter is most concentrated. The surface (A) horizon of the uppermost paleosol (Alfisol) examined in this work showed classic evidence of burial gleization with drab-colored mottles and tubular features predominantly in the A-horizon with minor radiation downward into the subsurface (Bt) horizon (Fig. 3) as well as accumulations of Fe^{2+} exclusively in the A-horizon (Table S1). Spectroscopic techniques such as VNIR employed here can readily identify burial gleization by observing absorbance features attributed to Fe^{2+} in the surface horizons of paleosols. This was presumably the cause of the broad $1.1\text{-}\mu\text{m}$ Fe^{2+} band in the surface of the Alfisol, and the shoulders at $2.23\text{--}2.25\ \mu\text{m}$ noted in the gleyed surface horizon of the Alfisol (Figs. 5 and 6).

Burial gleization can be distinguished from other original redoximorphic features such as groundwater alteration because it is limited to the surface (A) horizon unlike the gleyed subsurface (Bg) horizons of seasonally or perennially waterlogged soils, and because the mineralogy and morphology of this soil provide evidence of well-drained and oxidizing conditions during soil formation. Morphological evidence of burial gleization in paleosols is a drab greenish-gray color exclusively in near-surface horizons directly below the burial contact (PiPujol and Buurman, 1994). Geochemical evidence of burial gleization can include depletions of Fe^{3+} coupled with increases in Fe^{2+} and the formation of siderite and/or pyrite. Most soils accumulate organic matter in near-surface horizons, which after burial and the onset of anoxic conditions is generally the horizon most affected by burial gleization. Though the timing of burial gleization remains poorly constrained, reduction haloes around buried organic matter such as roots can form in tens to hundreds of years after burial (Allen, 1986). In the Alfisol, burial gleization can be distinguished from groundwater alteration because it is limited to the surface horizon directly below the white biotite-bearing tuff layer which buried the uppermost soil (Fig. 3). The original color of the surface horizon of the Alfisol was most likely brown and darkened by accumulation of organic matter. Burial gleization thus indicates the surface horizon of the Alfisol may be enriched in organic matter relative to unaffected subsurface horizons (Bt and C horizons), but burial degradation of organic carbon over geological time scales has likely reduced

the original organic carbon content by up to two orders of magnitude (Broz, 2020).

Directly below the drab surface horizon, the remainder of the Alfisol profile was brick-red in color (Fig. 3, Munsell 10R 3/1) which most likely resulted from dehydration of iron oxyhydroxides (Spinola et al., 2018). This phenomenon, also known as “burial reddening”, is one of the most common types of diagenetic alteration in the fossil record of soils on Earth (Retallack, 1991, 2019). Diagenetic dehydration of oxyhydroxides such as goethite and ferrihydrite forms strongly crystalline hematite which leads to reddening of soils that are originally brown or yellow in color; however, there is little information about the specific temperatures and pressures at which dehydration reactions occur (Spinola et al., 2018). Such a deep red color is unlikely to be the original color of the Alfisol because comparable modern Alfisols with smectite mineralogy are brown to yellow in color (Sheldon et al., 2002). Brown and yellow weakly to moderately developed Eocene paleosols from Antarctica also have deep red hues attributed to burial dehydration of ferrihydrite and goethite (Spinola et al., 2018). Some of the kaolinitic and lateritic paleosols in the Clarno and lower John Day Formations show evidence of deep weathering comparable to modern tropical soils that are red in color; however, soils that are not so deeply weathered such as the Alfisol examined here also have a brick-red color which is consistent with burial reddening. Other factors which cause reddening of paleosols include heating by lava flows (Sheldon, 2003) which can also cause iron oxyhydroxides to dehydrate to hematite and maghemite, but the effects of reddening are typically limited to the near-surface horizons due to the thermal insulation properties of soils (Solleiro-Rebolledo et al., 2016). Another possibility is that the protolith of the soil was red in color, but relict bedding and volcanic shards in the subsurface (C) horizon (Fig. 3) imply a tuffaceous parent material unlikely to be red in color.

The presence of clinoptilolite detected with XRD in all samples (Table 1) suggests zeolitization has pervasively altered paleosols from the John Day Formation. Though zeolites can form in alkaline volcanic soils (Ming and Mumpston, 1989), a diagenetic origin for clinoptilolite is likely because zeolites are commonly destroyed by hydrolysis during original soil formation, especially in the case of the moderately weathered, smectite-rich Alfisol. There are two proposed mechanisms of zeolitization to the John Day Formation paleosols. First, the aqueous flushing model of Hay (1963) proposed that volcanic glass in the lower John Day Formation was diagenetically altered to zeolites by open-system interactions with groundwater that added Ca and H₂O while removing Si, Na and K. Zeolitization may have occurred during early Miocene deep burial at depths of 380–1200 m and temperatures of 27–55 °C during deposition of the overlying Mascall and Rattlesnake Formations. Though the timing of zeolitization is well constrained, the mechanism of alteration by aqueous flushing is not likely because many silty tuff beds in the John Day Formation escaped zeolitization while the clay mineral-rich paleosols did not (Retallack et al., 2000). These permeable silty tuff beds would have presumably been channels for groundwater, but they include both zeolitized and non-zeolitized segments along strike, suggesting a more localized or patchy distribution of zeolitized facies. These observations are consistent with the hypothesis that some tuffs and paleosols were subject to zeolitization, while others were not.

Rather than zeolites forming from groundwater alteration, diagenesis may have been more localized and the formation of clinoptilolite may have instead resulted from burial-induced recrystallization of amorphous colloids and/or volcanic glass (Steefel and Van Cappellen, 1990; Chadwick and Chorover, 2001). The “burial ripening” model of Retallack et al. (2000) for zeolitization of paleosols is supported by observations of only small differences between abundances of alkali and alkali earths in paleosols most altered by zeolitization (the Turtle Cove Member paleosols) when compared with minimally altered tuffs. The stepwise increase in alkali and alkali earths in paleosols from the lower

John Day Formation to the upper Turtle Cove Member most likely resulted from decreases in weathering intensity during climatic cooling and drying and is independently supported by soil morphological and paleobotanical evidence of cooling and drying (Bestland, 1997; Retallack et al., 2000). Altogether these lines of evidence support the ripening model for zeolitization which led to localized formation of clinoptilolite from burial-induced crystallization of volcanic glass and/or amorphous colloids. The mechanism(s) of zeolitization are important for interpreting paleosols of the middle John Day Formation including those examined here because their chemical composition would be pervasively altered by the aqueous flushing model, whereas by the burial ripening model their original chemical composition would not have been significantly altered (Retallack et al., 2000).

Paleosols from the lower John Day formation are buried by approximately 2 km of overburden which has led to significant mechanical compaction. Burial of soil most often results in compaction of void spaces, fossils and pore water. In clayey soils such as those examined here, compaction of originally loose soil peds creates a complex pattern of slickensides with random orientation that resembles slickensides in modern smectitic soils with high shrink-swell capacity (Vertisols in US Taxonomy). Paleosols from the John Day Formation are geologically young enough to allow for comparisons with standard compaction curves for sedimentary rocks. Individual profiles from the middle Big Basin Member are covered by an additional 499 m of John Day formation, 305 m of Columbia River Basalt, up to 605 m of Mascall Formation, and 244 m of Rattlesnake Formation. From this overburden, compaction of paleosols can be estimated using the compaction curve of Sclater and Christie (1980) and are compacted to an estimated ~70% of their original thickness, which would suggest an original thickness of about 1.3 m for the uppermost Alfisol profile, 0.4 m for the Entisol profile, and 1.3 m for the lowermost Inceptisol profile.

3.6. Implications for Mars

Paleosols at the John Day Fossil Beds National Monument have been proposed to be comparable with putative weathering profiles on Mars because of similarities in mineralogy, morphology and stratigraphy (Horgan et al., 2012; Horgan, 2016; Hays et al., 2017; Broz, 2020). These sedimentary rocks can be used to help interpret the alteration history of sedimentary rocks on Mars. It should be noted that the paleosols of the Columbia River Basalt Group (~16 Ma), which are meter-scale paleosols that formed atop lava flows (e.g., Sheldon, 2003), might be a better analog for constraining the alteration history of martian lava flows. Critically, the protolith(s) of weathering profiles on Mars are not currently well constrained and could be exposed lava flows, tephra, sediments, or some combination of the three. The examination of terrestrial paleosols presented here, which formed in volcanic ash and lithic tuff, have implications for a) interpreting orbital remote sensing data for the pedogenic/diagenetic history of sedimentary rocks on Mars, b) interpreting in-situ results from Martian weathering profiles, and d) biosignature preservation in paleosols.

3.6.1. Orbital remote sensing

Orbital VNIR spectra can be compared with VNIR spectra from terrestrial paleosols to evaluate the pedogenic and diagenetic history of ancient sedimentary rocks on Mars. In-situ VNIR spectroscopy of multiple individual paleosol profiles presented here provides a reference frame for evaluating a pedogenic alteration hypothesis for ancient sedimentary rocks on Mars. Though pedogenic processes may have been ubiquitous across the surface of early Mars (Carter et al., 2015), it is currently unclear from orbital VNIR spectroscopy if weathering sequences formed from continuous pedogenic alteration (e.g., a deep weathering profile) (Liu et al., 2021a, 2021b), or if multiple episodes of alteration followed by burial occurred (e.g., repeated episodes of volcanic ash deposition, subaerial weathering, and burial) (Bishop et al.,

2018). The latter formation mechanism is characteristic of paleosol sequences that are composed of hundreds of individual paleosol profiles (Retallack, 2019) such as the Oregon paleosol sequence examined in the present study. At Mawrth Vallis, meter-scale relict bedding of the middle (α_2) Al-smectite stratigraphic unit at Muara Crater (Liu et al., 2021a) is consistent with a paleosol sequence hypothesis, though previous work has considered this unit part of a single, massive (~200 m-thick) deep weathering profile (Liu et al., 2021a). However, the apparent relict bedding of dark-toned layers in the α_2 unit (Lowe et al., 2020) would presumably be destroyed if the entire deposit was a deep weathering profile. Vertical changes in mineralogy at Muara Crater are consistent with changes in climate, weathering intensity and geochemistry rather than top-down leaching of acidic and reducing fluids through hundreds of vertical meters of stratigraphy. Furthermore, the resolution of CRISM poses challenges for distinguishing between a paleosol sequence and a deep weathering profile. The orbital remote sensing resolution of CRISM (typically 18 m/ pixel) (Murchie et al., 2007) is much coarser compared to our in-situ VNIR observations (sub-meter scale), which perhaps makes groups of individual paleosol profiles appear as “units” with similar mineralogy. Observations of the Oregon paleosol sequence suggest that changes in climate (e.g. Eocene-Oligocene cooling and drying) led to stratigraphic changes in mineralogy rather than the intense and uninterrupted leaching that is characteristic of a deep weathering profile. As such, the Oregon paleosol sequence reflects a cycle of continuous soil formation and burial that occurred during ~15 million years of climate change. These changes are reflected in the tens of individual paleosol profiles composing the basal Fe/Mg smectite and oxide unit (Clarno Formation, Fig. 1) that are overlain by hundreds of individual profiles with Al/Fe smectite mineralogy in the middle unit (Big Basin Member, John Day Formation) which are subsequently overlain by hundreds of profiles dominated by nanophase/amorphous Al and Si materials, hydrated silica, calcite and celadonite in the upper unit (Turtle Cover Member). This type of climate change and repeated soil formation may explain the compositional stratigraphy at Muara Crater, which currently stands as the best example of a putative paleosol sequence on Mars.

3.6.2. Interpreting in-situ rover data from future missions

The examination of Mars-analog paleosols can also help interpret the nature of aqueous alteration of rocks on Mars. Data from in-situ investigation of putative Mars weathering profiles can be compared to spectral and morphological features observed in this study to constrain pedogenic and diagenetic history of altered rocks. Pedogenic features observed in this work included strong VNIR absorbance bands characteristic of dioctahedral Al and Fe smectites; changes in clay mineralogy with depth, primarily observed in the 2.1–2.5 μm range; illuvial accumulation of clay minerals into subsurface (Bt) horizons; destruction of sedimentary bedding in weathered upper layers (A and B horizons); preservation of relict bedding in unweathered bottom layers (C horizons); and centimeter-scale changes in color and composition. These are all diagnostic features of terrestrial soils and should be considered permissive evidence of pedogenic alteration on Mars. Spectral features of diagenetic alterations included absorbances characteristic of zeolites and hematite. On Mars, these may indicate zeolitization and burial dehydration of iron (oxy)hydroxides, respectively. These and other forms of diagenesis are common in terrestrial paleosols that formed from weathering of volcanoclastic sediments (Retallack, 2019) buried by kilometers of overburden and may also explain occurrences of zeolites (Bishop and Rampe, 2016) and hematite (Liu et al., 2021b) detected from orbit in putative weathering sequences on Mars.

This study also provides a preliminary protocol for constraining climate and habitability from the geochemistry of weathering profiles on Mars. Molecular weathering ratios that have been well-studied in terrestrial paleosols (e.g., Sheldon et al., 2002; Liivamägi et al., 2018) could be useful for interpreting climate and habitability of weathering

profiles on Mars. By using a suite of molecular weathering ratios and geochemical climofunctions, a reconstruction of the climate and nature of weathering could be inferred from weathering profiles on Mars. However, differences in the nature of weathering and diagenesis between Earth and Mars present challenges for making direct comparisons. Such differences include a presumably anoxic early Mars atmosphere that perhaps led to Fe^{2+} mobility during subaerial weathering (Liu et al., 2021a), and the apparent absence of plate tectonics on Mars which has implications for the nature and severity of diagenesis of Noachian weathering profiles (Tosca and Knoll, 2009; Scheller et al., 2021).

One additional consideration is application of the chemical index of alteration to weathering profiles on Mars that may have been subject to weathering by acidic and sulfur-rich fluids. Weathering indices such as CIA may not accurately reflect acid sulfate weathering of mafic sediments because weathering rates of mafic materials such as olivine proceeds more efficiently than feldspars, especially under acidic conditions (Berger et al., 2017). Acidic conditions also affect the mobility of alkaline elements which may further confuse interpretations of weathering intensity by examining CIA (Liu et al., 2021b). Martian weathering profiles that appear to have been altered by fluids with circumneutral pH are better candidates for application of terrestrial molecular weathering ratios, weathering indices, and geochemical climofunctions. Alteration of mafic parent materials such as basalt may also be better assessed by the Mafic Index of Alteration (MIA) than by CIA (Babechuk et al., 2014). The redox-dependent mobility of Fe is factored into two variants of MIA that apply to oxidizing (MIA_O) and reducing (MIA_R) alteration conditions, as well as for extreme weathering conditions (e.g., the index of lateritisation) (Babechuk et al., 2014), that may be useful for constraining the alteration history of martian lava flows.

3.6.3. Biosignature preservation and detection in paleosols

The mineralogy and diagenetic alteration of terrestrial paleosols also has implications for biosignature preservation in Martian weathering profiles. Biosignatures in paleosols can include biomarkers, biominerals, macro and microstructures and textures, chemistry, and isotopes (Hays et al., 2017), and the rapid burial that characteristically entombs paleosols often creates favorable taphonomic environments for the preservation of biosignatures. Many factors contribute to the preservation and degradation of biosignatures in terrestrial paleosols. These include clay mineralogy, amorphous phase composition and abundance, diagenetic alterations, interactions with sulfur (e.g., sulfurization), and redox state prior to burial (Horgan et al., 2012; Broz, 2020). Redox state provides a first-order control on the preservation of organic carbon in rapidly buried soils (Broz, 2020). For example, soils forming under reducing conditions (e.g., wetlands) generally preserve higher abundances of organics relative to those forming in oxidized, well-drained conditions. Al-smectite rich soils, such as those examined in this study, have longer organic carbon residence time relative to soils with kaolin group clays (Wattel-Koekkoek et al., 2003), but well-drained, oxidizing conditions before burial are also associated with severe losses of organic C after burial (Retallack, 2019; Broz, 2020).

Most types of diagenetic alteration commonly observed in terrestrial paleosols are associated with the degradation of organic matter. Illitization, zeolitization and celadonization may facilitate desorption of organic carbon held on mineral surfaces, interlayer spaces, and crystal edges, thus possibly contributing to burial-induced degradation of organic matter (Elliott and Matisoff, 1996; Li et al., 2016). By contrast, several authors have reported that early diagenetic smectite-illite transformation may be facilitated by microbes themselves (Elliott and Matisoff, 1996; Fang et al., 2017; Becker-Kerber et al., 2021) which has implications for biosignature preservation in illite-rich soils. In this work, illitization and celadonization of smectite was not observed, but zeolitization of amorphous colloids and/or poorly crystalline smectite may have liberated adsorbed or chemisorbed organic carbon (Kaiser

and Guggenberger, 2000) and likely contributed to the degradation of the bulk organic fraction. One the other hand, diagenetic features of paleosols such as burial gleization observed in this work (Table S1 and Fig. 3) may indicate organic carbon enrichment and the preservation of chemical biosignatures in the near-surface horizons of paleosols. The drab green surface layer of the uppermost paleosol examined in this work showed an accumulation of Fe^{2+} attributed to diagenetic burial gleization via anaerobic microbial decay of organic matter. Previous investigations showed that this gleyed layer was enriched in organic carbon relative to deeper layers in the paleosol (Broz, 2020), and thus burial gleization features may constitute a chemical biosignature in paleosols. If features resembling burial gleization are detected in upper layers of weathering profiles on Mars, they should be considered a high-priority location for in-situ biosignature investigation.

4. Conclusions

A principal question of this research was whether the mineralogy and diagenetic alteration of terrestrial paleosols can be identified using techniques relevant to Mars exploration. The objective of this study was to determine the mineralogy and diagenetic alteration of Mars-analog paleosols from eastern Oregon, USA using analytical techniques similar to those onboard current and future missions to Mars.

Samples were gathered from three successive paleosol profiles in the early Oligocene (33 Ma) middle Big Basin Member of the John Day Formation. These profiles formed as a result of pedogenic weathering of andesitic to rhyodacitic volcanic ash and tuff. Visible/near infrared spectroscopy, X-ray diffraction and evolved gas analysis were suitable techniques for constraining the mineralogy and diagenesis of terrestrial paleosols. Together, these techniques confirmed dioctahedral smectite was the major phase in all samples, with most samples primarily containing a mixture of montmorillonite (Al smectite) and nontronite (Fe smectite). Minor phases detected with X-ray diffraction included Opal-CT, cristobalite, andesine and gypsum. All samples contained minor amounts of the zeolite mineral clinoptilolite which most likely formed from the diagenetic recrystallization of nanocrystalline phases such as allophane, imogolite and/or poorly crystalline smectite. Across all samples only minor (< 5 wt%) abundances of amorphous phases were observed; instead, most samples contained between 70 and 95 wt% crystalline clay minerals.

The mineralogy and morphology of paleosols examined here was consistent with formation under well-drained, oxidizing conditions with moderate weathering rates. Geochemical climofunctions based on molecular weathering ratios previously applied to these paleosols (Sheldon et al., 2002) indicated soil formation under mean annual precipitation of ~600 mm and mean annual temperature of approximately 10 °C. Pedogenic weathering of volcanic ash under these climatic conditions was sufficient to transform volcanic glass and amorphous/nanocrystalline phases into strongly crystalline dioctahedral clay minerals.

Four types of alteration after burial that have affected paleosols examined in this work are 1) drab green surface horizons due to burial gleization of organic matter; 2) brick-red color from burial-induced dehydration of ferric oxides and hydroxides; 3) zeolitization of volcanic glass and/or poorly crystalline phases; and 4) significant mechanical compaction. Burial gleization, limited to the surface horizons of paleosols, was most likely an early diagenetic alteration that resulted from the chemical reduction of iron hydroxides and oxides by anaerobic bacteria consuming buried organic matter at or below the water table. The timing of burial dehydration of (oxy)hydroxides remains poorly constrained, but late diagenetic alterations such as zeolitization may have occurred during early Miocene burial at depths of 380 to 1200 m and temperatures of 27–55 °C during deposition of the overlying Mascall and Rattlesnake Formations. The current overburden of ~2 km has also resulted in the mechanical compaction of paleosol profiles to approxi-

mately 70% of their original thickness before burial. Despite significant overburden, absence of illite/chlorite and celadonite imply a lack of diagenetic K-metasomism and celadonization, respectively. The high clay mineral content (up to 95 wt%) of paleosols from the middle Big Basin Member of the John Day Formation may have insulated profiles from diagenetic alterations which have pervasively altered stratigraphically higher and less clay mineral-rich (~40 wt%) paleosols in the overlying Turtle Cove member of the John Day Formation.

On Mars, there are distinct stratigraphic changes in clay and amorphous phase abundance in sedimentary rocks across the Mawrth Vallis region. These general stratigraphic trends have also been observed in the eastern Oregon paleosol sequence. Mineralogical changes across the compositional stratigraphy at Muara Crater, Mawrth Vallis is comparable to the up-section decline in crystalline clay minerals and subsequent increase in Al smectite, amorphous phases and hydrated silica through the Clarno and John Day Formations resulting from the aridification of eastern Oregon during the late Eocene and Oligocene. Strong spectral signatures of a nanophase aluminosilicate consistent with allophane and/or imogolite have been noted at the stratigraphically highest layers across the Mawrth Vallis region and are thought to represent a cool and dry climate where nanophase aluminosilicates resulted from minor alteration of volcanic ash (Bishop et al., 2016). These uppermost layers of the Mawrth Vallis stratigraphy appear to share mineralogical similarities with the terrestrial Turtle Cove Member paleosols. In contrast, the lowermost layers at Mawrth Vallis have strong spectral signatures of crystalline Fe/Mg smectite and are perhaps more akin to deeply weathered paleosols from the Clarno and lower John Day Formations.

Pedogenic features observed in this work include dioctahedral smectite mineralogy, a clay mineral doublet feature observed with VNIR spectroscopy that may have been a result of isomorphous substitutions during pedogenic weathering, the destruction of sedimentary bedding, sub-meter scale differences in composition and color, and the illuvial accumulation of clay minerals into subsurface horizons. All of the above features resulted from precipitation-driven pedogenic weathering of andesitic to rhyodacitic volcanic ash and tuff. Results from this work can help distinguish paleosols and weathering profiles from other types of sedimentary rocks in the geological record of Mars.

Author contribution statement

A.P.B designed the study, performed laboratory analyses, and drafted the manuscript. B.H.H identified similarities between Mars and John Day paleosols, assisted with fieldwork and provided VNIR spectra of paleosols. J.V.C guided all thermal analyses and facilitated data interpretation. B.S, J.V.C and D.W.M performed data analysis and interpretation. V.T. conducted x-ray diffraction and assisted with interpretation of mineralogy. L.C.R.S supervised the project. All authors contributed to the manuscript.

Author disclosure statement

No competing financial interests exist.

Declaration of Competing Interest

None.

Acknowledgements

This work was performed on the ancestral homelands of the Numu, Cayuse, Umatilla, Walla Walla, and Confederated Tribes of the Warm Springs who were present before western settlement. Many thanks to Elizabeth Rampe and Paul Niles for the opportunity to work on this project and for providing research direction during a summer internship. This project was part of a PhD dissertation supervised by Greg Retallack

and Lucas C.R Silva. Barry Hughes and Megan Barrington assisted with fieldwork and entertained thoughtful discussion. Anais Roussel, Angela Olsen, Marshall Styczinski, Paul Regensberger and Joe Caggiano reviewed early versions of the manuscript. Funding from the Geological Society of America, The National Science Foundation, The Clay Minerals Society, The Society of Sedimentary Geology, and the Central Oregon Geoscience Society aided in the completion of this project.

Appendix A. Supplementary data

Supplementary data to this article can be found online at <https://doi.org/10.1016/j.icarus.2022.114965>.

References

- Allen, J.R.L., 1986. Time scales of colour change in late Flandrian intertidal muddy sediments of the Severn estuary. *Proc. Geol. Assoc.* 97, 23–28. [https://doi.org/10.1016/S0016-7878\(86\)80002-5](https://doi.org/10.1016/S0016-7878(86)80002-5).
- Babechuk, M.G., Widdowson, M., Kamber, B.S., 2014. Quantifying chemical weathering intensity and trace element release from two contrasting basalt profiles, Deccan Traps, India. *Chem. Geol.* 363, 56–75. <https://doi.org/10.1016/j.chemgeo.2013.10.027>.
- Barrington, M., Tate, C.D., Hayes, A., Bell, J., Horgan, B., Rice, M., 2020. Mastcam-Z Analog Spectral Imager: 51st Lunar and Planetary Science Conference. 1595. pp. 51–52.
- Becker-Kerber, B., et al., 2021. The role of volcanic-derived clays in the preservation of Ediacaran biota from the Itajaí Basin (ca. 563 Ma, Brazil). *Sci. Rep.* 11, 1–10. <https://doi.org/10.1038/s41598-021-84433-0>.
- Berger, J.A., et al., 2017. Zinc and germanium in the sedimentary rocks of Gale Crater on Mars indicate hydrothermal enrichment followed by diagenetic fractionation. *J. Geophys. Res. Planet.* 1747–1772. <https://doi.org/10.1002/2017JE005290>.
- Bestland, E., 1997. Alluvial terraces and paleosols as indicators of early Oligocene climate change (John-Day Formation, Oregon). *J. Sediment. Res.* 67, 840–855. <https://doi.org/10.1306/D4268653-2B26-11D7-8648000102C1865D>.
- Bestland, E.A., 2002. Fossil Andisols identified with mass-balance geochemistry (Oligocene John Day Formation, Oregon, U.S.A.). *J. Sediment. Res.* 72, 673–686. <https://doi.org/10.1306/021802720673>.
- Beukes, N.J., Dorland, H., Nedachi, M., Ohmoto, H., 2002. Tropical laterites, life on land and the history of atmospheric oxygen in the Paleoproterozoic. *Geology* 30, 491–494.
- Bishop, J.L., Rampe, E.B., 2016. Evidence for a changing Martian climate from the mineralogy at Mawrth Vallis. *Earth Planet. Sci. Lett.* 448, 42–48. <https://doi.org/10.1016/j.epsl.2016.04.031>.
- Bishop, J.L., Lane, M.D., Dyar, M.D., Brown, A.J., 2008a. Reflectance and emission spectroscopy study of four groups of phyllosilicates: smectites, kaolinite-serpentines, chlorites and micas. *Clay Miner.* 43, 35–54. <https://doi.org/10.1180/claymin.2008.043.1.03>.
- Bishop, J., et al., 2008b. Phyllosilicate diversity and past aqueous activity revealed at Mawrth Vallis, Mars. *Science* 830–834.
- Bishop, J.L., Loizeau, D., Mckeown, N.K., Saper, L., Dyar, M.D., Des, D.J., Parente, M., Murchie, S.L., 2013. What the ancient phyllosilicates at Mawrth Vallis can tell us about possible habitability on early Mars. *Planet. Space Sci.* 86, 130–149. <https://doi.org/10.1016/j.pss.2013.05.006>.
- Bishop, J., et al., 2016. Mineralogy of layered outcrops at Mawrth Vallis and implications for early aqueous geochemistry on Mars. In: 47th Lunar and Planetary Science Conference, 2, pp. 2–3. <https://doi.org/10.1002/2014JE004627>.
- Bishop, J.L., Fairén, A.G., Michalski, J.R., Gago-duport, L., Baker, L.L., Velbel, M.A., Gross, C., Rampe, E.B., 2018. Surface clay formation during short-term warmer and wetter conditions on a largely cold ancient Mars. *Nat. Astr.* 2, 206–213. <https://doi.org/10.1038/s41550-017-0377-9>.
- Bishop, J.L., Gross, C., Danielsen, J., Parente, M., Murchie, S.L., Horgan, B., Wray, J.J., Viviano, C., Seelos, F.P., 2020. Multiple mineral horizons in layered outcrops at Mawrth Vallis, Mars, signify changing geochemical environments on early Mars. *Icarus* 341, 113634. <https://doi.org/10.1016/j.icarus.2020.113634>.
- Breecker, D.O., Sharp, Z.D., McFadden, L.D., 2009. Seasonal bias in the formation and stable isotopic composition of pedogenic carbonate in modern soils from Central New Mexico, USA. *Bull. Geol. Soc. Am.* 121, 630–640. <https://doi.org/10.1130/B26413.1>.
- Bristow, T.F., et al., 2018. Clay mineral diversity and abundance in sedimentary rocks of Gale crater. *Mars. Sci. Adv.* 4, 1–9.
- Broz, A.P., 2020. Organic matter preservation in ancient soils of earth and Mars. *Life* 10. <https://doi.org/10.3390/life10070113>.
- Bultel, B., Viennet, J.C., Poulet, F., Carter, J., Werner, S.C., 2019. Detection of carbonates in Martian weathering profiles. *J. Geophys. Res. Planet.* 124, 989–1007. <https://doi.org/10.1029/2018JE005845>.
- Butt, C.R.M., Lintern, M.J., Anand, R.R., 2000. Evolution of regoliths and landscapes in deeply weathered terrain — implications for geochemical exploration. *Ord. Geol. Rev.* 16, 167–183.
- Cannon, K.M., Stephen, W., Mustard, J., 2017. Primordial clays on Mars formed beneath a steam or supercritical atmosphere. *Nature* 552, 88–91. <https://doi.org/10.1038/nature24657>.
- Carter, J., Loizeau, D., Mangold, N., Poulet, F., Bibring, J., 2015. Widespread surface weathering on early Mars : a case for a warmer and wetter climate. *Icarus* 248, 373–382. <https://doi.org/10.1016/j.icarus.2014.11.011>.
- Chadwick, O.A., Chorover, J., 2001. The chemistry of pedogenic thresholds. *Geoderma* 100, 321–353. [https://doi.org/10.1016/S0016-7061\(01\)00027-1](https://doi.org/10.1016/S0016-7061(01)00027-1).
- Chemtob, S.M., Nickerson, R.D., Morris, R.V., Agresti, D.G., Catalano, J.G., 2015. Synthesis and structural characterization of ferrous trioctahedral smectites: implications for clay mineral genesis and detectability on Mars. *J. Geophys. Res. E Planet.* 120, 1119–1140. <https://doi.org/10.1002/2014JE004763>.
- Chipera, S.J., Bish, D.L., 2001. Baseline studies of the clay minerals society source clays: colloid and surface phenomena. *Clay Clay Miner.* 49, 446–452. <https://doi.org/10.1346/CCMN.2001.0490511>.
- Danielson, J., Bishop, J., Usabel, G.S., Miura, J., Sessa, A., Wray, J., Itoh, Y., Parente, M., Murchie, S., 2019. Characterization of outcrops containing “doublet” spectra at Mawrth Vallis, Mars. In: Lunar and Planetary Science Conference, 2019, pp. 1–179. <https://doi.org/10.1029/2008g>.
- Dobrea, E.Z.N., et al., 2010. Mineralogy and stratigraphy of phyllosilicate - bearing and dark mantling units in the greater Mawrth Vallis / west Arabia Terra area : constraints on geological origin. *J. Geophys. Res.* 115, 1–27. <https://doi.org/10.1029/2009JE003351>.
- Driese, S.G., Ober, E.G., 2005. Paleopedologic and paleohydrologic records of precipitation seasonality from early Pennsylvanian “underclay” paleosols, U.S.a. *J. Sediment. Res.* 75, 997–1010. <https://doi.org/10.2110/jsr.2005.075>.
- Earnest, C.M., 1991. Thermal analysis of selected illite and smectite clay minerals. Part II. Smectite clay minerals. In: Smykatz-Kloss, W., Warne, S.S.J. (Eds.), *Thermal Analysis in the Geosciences*. Springer Berlin Heidelberg, Berlin, Heidelberg, pp. 288–312.
- Ehlmann, B.L., Mustard, J.F., Fassett, C.I., Schon, S.C., Iii, J.W.H., Marais, D.J.E.S., Grant, J.A., Murchie, S.L., 2008. Clay minerals in delta deposits and organic preservation potential on Mars. *Nature* 1, 355–358. <https://doi.org/10.1038/ngeo207>.
- Ehlmann, B.L., Mustard, J.F., Murchie, S.L., 2010. Geologic setting of serpentine deposits on Mars. *Geophys. Res. Lett.* 37, 1–5. <https://doi.org/10.1029/2010GL042596>.
- Ehlmann, B.L., Mustard, J.F., Murchie, S.L., Bibring, J., Meunier, A., Fraeman, A.A., Langevin, Y., 2011. Subsurface water and clay mineral formation during the early history of Mars. *Nature* 479, 53–60. <https://doi.org/10.1038/nature10582>.
- Elliott, W.C., Matisoff, G., 1996. Evaluation of kinetic models for the smectite to illite transformation. *Clay Clay Miner.* 44, 77–87. <https://doi.org/10.1346/CCMN.1996.0440107>.
- Fang, Q., Churchman, G.J., Hong, H., Chen, Z., Liu, J., Yu, J., Han, W., Wang, C., Zhao, L., Furnes, H., 2017. Applied clay science new insights into microbial smectite illitization in the Permo-Triassic. *Appl. Clay Sci.* 140, 96–111. <https://doi.org/10.1016/j.clay.2017.01.029>.
- François, P., Szopa, C., Buch, A., Coll, P., Mcadam, A.C., Mahaffy, P.R., Freissinet, C., Glavin, D.P., Cabane, M., 2015. Magnesium sulfate as a key mineral for the detection of organic molecules on Mars using pyrolysis. *J. Geophys. Res. Planet.* 61–74. <https://doi.org/10.1002/2015JE004884>. Received.
- Franklin, R., et al., 2021. Oxia planum : the landing site for the ExoMars. *Astrobiology* 21, 1–22. <https://doi.org/10.1089/ast.2019.2191>.
- Goesmann, F., et al., 2017. The Mars organic molecule analyzer (MOMA) instrument: characterization of organic material in Martian sediments. *Astrobiology* 17, 655–685. <https://doi.org/10.1089/ast.2016.1551>.
- Hay, R., 1963. *Stratigraphy and Zeolitic Diagenesis of the John Day Formation of Oregon*. 42. pp. 199–252.
- Hays, L.E., Graham, H.V., Des Marais, D.J., Hausrath, E.M., Horgan, B., McCollom, T.M., Parente, M.N., Potter-McIntyre, S.L., Williams, A.J., Lynch, K.L., 2017. Biosignature preservation and detection in Mars analog environments. *Astrobiology* 17, 363–400. <https://doi.org/10.1089/ast.2016.1627>.
- Heard, A.W., Kite, E.S., 2020. A probabilistic case for a large missing carbon sink on Mars after 3.5 billion years ago. *Earth Planet. Sci. Lett.* 531, 116001. <https://doi.org/10.1016/j.epsl.2019.116001>.
- Heard, A.W., Aarons, S.M., Hofmann, A., He, X., Ireland, T., Bekker, A., Qin, L., Dauphas, N., 2021. Anoxic continental surface weathering recorded by the 2.95 Ga Denny Dalton Paleosol (Pongola Supergroup, South Africa). *Geochim. Cosmochim. Acta* 295, 1–23. <https://doi.org/10.1016/j.gca.2020.12.005>.
- Hogancamp, J.V., Ming, D.W., McAdam, A., Archer, P., Morris, R.V., Bristow, T.F., Rampe, E.B., Mahaffy, P.R., Gellert, R., 2017. Identification of phyllosilicates in mudstone samples using water releases detected by the Sample Analysis at Mars (SAM) instrument in Gale Crater, Mars. In: Lunar and Planetary Science XLVIII. p. 1620. <https://doi.org/10.1126/science.1243480>.
- Horgan, B.H.N., 2013. Climate change and a sequence of habitable ancient surface environments preserved in pedogenically altered sediments at Mawrth Vallis, Mars. In: *Lunar and Planetary Science Conference*. p. 3059.
- Horgan, B., 2016. Strategies for Searching for Biosignatures in Ancient Martian Sub-Aerial Surface Environments: Biosignature Preservation and Detection in Mars Analog Environments. p. 7463. <https://doi.org/10.1089/ast.2016.1627>.
- Horgan, B., Christensen, P., Iii, J.F.B., 2011. Searching for Pedogenic Phyllosilicates in Ancient Martian Soils: AGU Fall Meeting. p. 1999.
- Horgan, B., Bishop, L., Christensen, P.R., Bell, J.F., 2012. Potential ancient soils preserved at Mawrth Vallis from comparisons with Eastern Oregon paleosols: Implications for Early Martian Climate. In: *Third Conference on Early Mars*, 7074, pp. 12–13.
- Horgan, B., Baker, L., Carter, J., Chadwick, O., 2017a. Where is the climate signature in the mineral record of early Mars? In: *Fourth Conference on Early Mars 2017*, v, 3077, pp. 2014–2015. <https://doi.org/10.1038/ncomms15978>.
- Horgan, B., Fraeman, A., Rice, M., Bell, J., Wellington, D., Johnson, J., 2017b. New constraints from CRISM and MASTCAM spectra on the mineralogy and origin of Mt. Sharp geologic units, Gale Crater, Mars. In: *48th Lunar and Planetary Science Conference*, 3021, pp. 2–3.
- Horgan, B., Smith, R., Chadwick, O., Retallick, G., Dobrea, E.N., Christensen, P., 2017c.

- The effects of climate, environment, and diagenesis on the spectral properties of volcanic soils. In: GSA Annual Meeting, Cordilleran Section. pp. 1–24.
- Jones, R.C., Babcock, C.J., Knowlton, W.B., 2000. Estimation of the total amorphous content of Hawai'i soils by the Rietveld method. *Soil Sci. Soc. Am. J.* 1108, 1100–1108. <https://doi.org/10.2136/sssaj2000.6431100x>.
- Kaiser, K., Guggenberger, G., 2000. The role of DOM sorption to mineral surfaces in the preservation of organic matter in soils. *Org. Geochem.* 31, 711–725.
- Lantz, C., Poulet, F., Loizeau, D., Riu, L., Pilorget, C., Carter, J., Dypvik, H., Rull, F., Werner, S.C., 2020. Planetary terrestrial analogues library project: 1. Characterization of samples by near-infrared point spectrometer. *Planet. Space Sci.* 189, 104989. <https://doi.org/10.1016/j.pss.2020.104989>.
- Le Deit, L., Flahaut, J., Quantin, C., Hauber, E., Mège, D., Bourgeois, O., Gurgurewicz, J., Massé, M., Jaumann, R., 2012. Extensive surface pedogenic alteration of the Martian Noachian crust suggested by plateau phyllosilicates around Valles Marineris. *J. Geophys. Res.* 117, 1–25. <https://doi.org/10.1029/2011JE003983>.
- Li, Y., Cai, J., Song, M., Ji, J., Bao, Y., 2016. Influence of organic matter on smectite illitization: a comparison between red and dark mudstones from the Dongying Depression, China. *Am. Mineral.* 101, 134–145.
- Liivamägi, S., Rodón, J., Bojanowski, M., Gerdes, A., Stanek, J.J., Williams, L., Szczerba, M., 2018. Paleosols on the Ediacaran basalts of the East European craton: a unique record of paleoweathering with minimum diagenetic overprint. *Precambrian Res.* <https://doi.org/10.1016/j.precamres.2018.07.020>.
- Liu, J., Michalski, J.R., Tan, W., He, H., Ye, B., Xiao, L., 2021a. Anoxic chemical weathering under a reducing greenhouse on early Mars. *Nat. Astr.* <https://doi.org/10.1038/s41550-021-01303-5>.
- Liu, J., Michalski, J.R., Zhou, M., 2021b. Intense subaerial weathering of eolian sediments in Gale crater, Mars. *Sci. Adv.* 7. <https://doi.org/10.1126/sciadv.abb2687>.
- Loizeau, D., Mangold, N., Poulet, F., Bibring, J., Bishop, J.L., Michalski, J., Quantin, C., 2015. History of the clay-rich unit at Mawrth Vallis, Mars: high-resolution mapping of a candidate landing site. *J. Geophys. Res. Planet* 1820–1846. <https://doi.org/10.1002/2015JE004894>. Received.
- Loizeau, D., Quantin-nataf, C., Carter, J., Flahaut, J., Thollot, P., Lozac, L., Millot, C., 2018. Quantifying widespread aqueous surface weathering on Mars: the plateaus south of Coprates Chasma. *Icarus* 302, 451–469. <https://doi.org/10.1016/j.icarus.2017.11.002>.
- Lowe, D.R., Bishop, J.L., Loizeau, D., Wray, J.J., Beyer, R.A., View, M., 2020. Deposition of > 3.7 Ga clay-rich strata of the Mawrth Vallis Group, Mars, in lacustrine, alluvial, and aeolian environments. *GSA Bull.* 17–30.
- Lukens, W.E., Nordt, L.C., Stinchcomb, G.E., Driese, S.G., Tubbs, J.D., 2018. Reconstructing pH of paleosols using geochemical proxies. *J. Geol.* 126, 427–449. <https://doi.org/10.1086/697693>.
- Mahaffy, P.R., et al., 2012. The sample analysis at Mars investigation and instrument suite. *Space Sci. Rev.* 170, 401–478. <https://doi.org/10.1007/s11214-012-9879-z>.
- McAdam, A., et al., 2014. Sulfur-bearing phases detected by evolved gas analysis of the Rocknest aeolian deposit, Gale Crater, Mars. *J. Geophys. Res. Planet* 119, 6121–6139. <https://doi.org/10.1002/2013JE004518>. Received.
- McAdam, A., et al., 2017. Constraints on Gale Crater mudstone from MSL SAM evolved water. In: *Lunar and Planetary Science XLVIII*. pp. 7–8. <https://doi.org/10.1126/science.1245267>.
- McAdam, A., Sutter, B., Archer, P., Franz, H., Eigenbrode, J., 2020. The chemistry and mineralogy of the Glen Torridon clay-bearing unit from Mars Science Laboratory Sample Analysis at Mars. In: *51st Lunar and Planetary Science Conference*, 2243, pp. 60–74.
- Michalski, J.R., Cuadros, J., Bishop, J.L., Dyar, M.D., Dekov, V., Fiore, S., 2015. Constraints on the crystal-chemistry of Fe/mg-rich smectitic clays on Mars and links to global alteration trends. *Earth Planet. Sci. Lett.* 427, 215–225. <https://doi.org/10.1016/j.epsl.2015.06.020>.
- Milliken, R., Mustard, J., Ehlmann, B.L., Bishop, J.L., Murchie, S.L., 2008. Interpreting and constraining the compositional and depositional environments of phyllosilicates on Mars. *Ground Truth From Mars* 4036, 7–8.
- Ming, D.W., Mumpston, F., 1989. Zeolites in soils. In: *Minerals in Soil Environments*, 18, pp. 873–911.
- Ming, D.W., et al., 2014. Volatile and Organic Compositions of Sedimentary Rocks in Yellowknife Bay, Gale Crater, Mars. *Sci. Expr.* 1–15. <https://doi.org/10.1126/science.1245267>.
- Morris, R.V., et al., 2016. Silicic volcanism on Mars evidenced by tridymite in high-SiO₂ sedimentary rock at Gale crater. *Proc. Natl. Acad. Sci. U. S. A.* 113, 7071–7076. <https://doi.org/10.1073/pnas.1607098113>.
- Murchie, S., et al., 2007. Compact reconnaissance imaging spectrometer for Mars (CRISM) on Mars reconnaissance orbiter (MRO). *J. Geophys. Res.* 112, 1–57. <https://doi.org/10.1029/2006JE002682>.
- Novoselov, A.A., Roberto, C., Filho, D.S., 2015. Potassium metasomatism of Precambrian paleosols. *Precambrian Res.* 262, 67–83. <https://doi.org/10.1016/j.precamres.2015.02.024>.
- PiPujol, M.D., Buurman, P., 1994. The distinction between ground-water gley and surface-water gley phenomena in Tertiary paleosols of the Ebro basin, NE Spain. *Palaeogeogr. Palaeoclimatol. Palaeoecol.* 110, 103–113. [https://doi.org/10.1016/0031-0182\(94\)90112-0](https://doi.org/10.1016/0031-0182(94)90112-0).
- Quantin, C., et al., 2016. Oxia Planum, the landing site for Exomars 2018. In: *47th Lunar and Planetary Science Conference*. p. 2863. <https://www.hou.usra.edu/meetings/lpsc2016/pdf/2863.pdf>.
- Quantin-Nataf, C., et al., 2021. Oxia planum: the landing site for the ExoMars “rosalind Franklin” rover mission: geological context and prelanding interpretation. *Astrobiology* 21, 345–366. <https://doi.org/10.1089/ast.2019.2191>.
- Rampe, E.B., et al., 2020. Mineralogy and geochemistry of sedimentary rocks and eolian sediments in Gale crater, Mars: a review after six Earth years of exploration with curiosity. *Geochemistry* 80. <https://doi.org/10.1016/j.chemer.2020.125605>.
- Retallack, G.J., 1991. Untangling the effects of burial alteration and ancient soil formation. *Annu. Rev. Earth Planet. Sci.* 183–206.
- Retallack, G.J., 1995. Paleosols of the Siwalik Group as a 15 Myr record of South Asian palaeoclimate. *Mem. Geol. Soc. India* 32, 36–51.
- Retallack, G.J., 2014. Paleosols and paleoenvironments of early Mars. *Geology* 42, 755–758. <https://doi.org/10.1130/G35912.1>.
- Retallack, G.J., 2019. *Soil of the Past*. Wiley Blackwell.
- Retallack, G.J., Bestland, E., Fremd, T., 2000. Eocene and Oligocene Paleosols of Central Oregon. *Geol. Soc. Am. Spec. Pap.* 344, 1–192. <https://doi.org/10.1046/j.1365-3091.2001.0394c.x>.
- Retallack, G.J., Martin, J.E., Broz, A.P., Breithaupt, B.H., Matthews, A., Walton, D.P., 2018. Late Pleistocene mammoth trackway from Fossil Lake, Oregon. *Paleogeogr. Paleoclimatol. Paleoecol.* <https://doi.org/10.1016/j.palaeo.2018.01.037>.
- Rye, R., Geological, D., Sciences, P., 2000. Life associated with a 2.76 Ga ephemeral pond? evidence from Mount Roe # 2 paleosol. *Geology* 483–486.
- Scheller, E.L., Ehlmann, B.L., Hu, R., Adams, D.J., Yung, Y.L., 2021. Long-term drying of Mars by sequestration of ocean-scale volumes of water in the crust. *Science* 372, 56–62. <https://doi.org/10.1126/science.abc7717>.
- Scatcher, J.G., Christie, P., 1980. Continental stretching: an explanation of the post-midcretaceous subsidence of the Central North Sea Basin. *J. Geophys. Res.* 85, 3711–3739. <https://doi.org/10.1029/JB085iB07p03711>.
- Sheldon, N.D., 2003. Pedogenesis and geochemical alteration of the Picture Gorge subgroup of the Columbia River basalt, Oregon. *Bull. Geol. Soc. Am.* 115, 1377–1387. <https://doi.org/10.1130/B25223.1>.
- Sheldon, N.D., Retallack, G.J., Tanaka, S., 2002. Geochemical Climofunctions from North American soils and application to paleosols across the Eocene–Oligocene boundary in Oregon geochemical climofunctions from North American soils and application to paleosols across the Eocene–Oligocene boundary in or. *J. Geol.* 110, 687–696. <https://doi.org/10.1086/342865>.
- Smith, R., Horgan, B.H.N., 2021. Nanoscale variations in natural amorphous and nanocrystalline weathering products in mafic to intermediate volcanic terrains on earth: implications for amorphous detections on Mars. *J. Geophys. Res. Planet* 126, 1–30. <https://doi.org/10.1029/2020JE006769>.
- Smith, R., Horgan, B., Rampe, E., Dehouck, E., 2018a. The composition of amorphous phases in soils and sediments on earth and Mars. In: *49th Lunar and Planetary Science Conference 2018*. pp. 14–15.
- Smith, R.J., Rampe, E.B., Horgan, B.H.N., Dehouck, E., 2018b. Deriving amorphous component abundance and composition of rocks and sediments on earth and Mars. *J. Geophys. Res. Planet* 123, 2485–2505. <https://doi.org/10.1029/2018JE005612>.
- Solleiro-Rebolledo, E., Straubinger, M., Terhorst, B., Sedov, S., Ibarra, G., Sánchez-Alaniz, J.I., Solanes, M.C., Marmolejo, E., 2016. Paleosols beneath a lava flow in the southern basin of Mexico: the effect of heat on the paleopedological record. *Catena* 137, 622–634. <https://doi.org/10.1016/j.catena.2014.12.002>.
- Spinola, D.N., de Portes, R.C., Srivastava, P., Torrent, J., Barrón, V., Kühn, P., 2018. Diagenetic reddening of Early Eocene paleosols on King George Island, Antarctica. *Geoderma* 315, 149–159. <https://doi.org/10.1016/j.geoderma.2017.11.010>.
- Staff, S.S., 2014. *Keys to Soil Taxonomy*. 12. Department of Agriculture, United States.
- Steeff, C.I., Van Cappellen, P., 1990. A new kinetic approach to modeling water-rock interaction: the role of nucleation, precursors, and Ostwald ripening. *Geochim. Cosmochim. Acta* 54, 2657–2677. [https://doi.org/10.1016/0016-7037\(90\)90003-4](https://doi.org/10.1016/0016-7037(90)90003-4).
- Sutter, B., Laurer, H., Golden, D., Ming, D., Boynton, W., 2008. Phoenix Lander's thermal evolved gas analyzer: Differential scanning calorimeter and mass spectrometer database development. In: *35th Lunar and Planetary Science Conference*, 21, pp. 1–3. <http://adsabs.harvard.edu/abs/2004LP...35.1964W>.
- Sutter, B., McAdam, A., Mahaffy, P., Ming, D., Edgett, K., Rampe, E., Eigenbrode, J., Franz, H., Freissinet, C., 2017. Evolved gas analyses of sedimentary rocks and eolian sediment in Gale Crater, Mars: results of the Curiosity rover's sample analysis at Mars instrument from Yellowknife Bay to the Namib Dune. *J. Geophys. Res. Planet* 2574–2609. <https://doi.org/10.1002/2016JE005225>.
- Tosca, N.J., Knoll, A.H., 2009. Juvenile chemical sediments and the long term persistence of water at the surface of Mars. *Earth Planet. Sci. Lett.* 286, 379–386. <https://doi.org/10.1016/j.epsl.2009.07.004>.
- Vaniman, D.T., Bish, D.L., Ming, D.W., Bristow, T.F., Morris, R.V., Blake, D.F., Chipera, S.J., 2014. Mineralogy of a Mudstone at Yellowknife Bay, Gale Crater, Mars mineralogical analysis and quantitative mineralogy. *Science* 1–14. <https://doi.org/10.1126/science.1243480>.
- Watanabe, Y., Martin, J.E., Ohmoto, H., 2000. Geochemical evidence for terrestrial ecosystems 2.6 billion years ago. *Nature* 408. <https://doi.org/10.1038/35046052>.
- Watanabe, Y., Stewart, B.W., Ohmoto, H., 2004. Organic- and carbonate-rich soil formation ~2.6 billion years ago at Schagen, East Transvaal district, South Africa. *Geochim. Cosmochim. Acta* 68, 2129–2151. <https://doi.org/10.1016/j.gca.2003.10.036>.
- Wattel-Koekkoek, E., Buurman, P., Van der Plicht, J., Wattel, E., van Breeman, N., 2003. Mean residence time of soil organic matter associated with kaolinite and smectite. *Eur. J. Soil Sci.* 54, 269–278. <https://doi.org/10.1046/j.1365-2389.2003.00512.x>.
- Yant, M., Young, K., Rogers, A., McAdam, A.C., Bleacher, J., Bishop, J.L., Mertzman, S.A., 2018. Visible, near-infrared, and mid-infrared spectral characterization of Hawaiian fumarolic alteration near Kilauea's December 1974 flow: implications for spectral discrimination of alteration environments on Mars. *Am. Mineral.* 103.
- Ye, B., Michalski, J.R., 2021. Precipitation-driven pedogenic weathering of volcanoclastics on early Mars. *Geophys. Res. Lett.* 48, 1–10. <https://doi.org/10.1029/2020GL091551>.
- Zauyah, S., Schaefer, C.E.G.R., Simas, F.N.B., 2018. Sapolites. Elsevier B.V., pp. 37–57. <https://doi.org/10.1016/b978-0-444-63522-8.00003-6>.